Table I. Antibodies for flow cytometry.

Antigen	Label	Manufacturer	Catalog number
CD11b	FITC	Beckman Coulter	IM1284
CD14	FITC	Beckman Coulter	IM0645
CD19	FITC	Beckman Coulter	IM1284
CD29	FITC	Beckman Coulter	6604105
CD31	FITC	BD	555445
CD34	PC7	Beckman Coulter	A21691
CD34	PC5	Beckman Coulter	A07777
CD38	FITC	Beckman Coulter	IM0775
CD44	PE[a]	Beckman Coulter	IM0845
CD45	FITC	Beckman Coulter	A07782
CD45	ECD	Beckman Coulter	A07784
CD73	Biotin[b]	BD	550256
CD90	PE	Beckman Coulter	IM1840
CD105	PE	Beckman Coulter	A07414
CD117	PE	Beckman Coulter	IM2732
CD133	PE	Miltenyi Biotec	130-080-901
GlycophorinA	PE	Beckman Coulter	IM2211
HLA-DR	FITC	BD	555560
vWF	FITC*	Beckman Coulter	IM0150

[a]Antibody was labeled with a Zenon Mouse IgG1 labeling kit (Invitrogen).
[b]Biotin-labeled antibody was detected by strept avidin–PC5.
FITC, fluorescein isothiocyanate; PE, phycoerythrin; PC, phycoerythrin-cyanin; ECD, phycoerythrin-TexasRED. BD, Becton Dickinson, Franklin Lakes, NJ, USA, Mitenyi Biotec; Bergisch Gladbach, Nordrhein-Westfalen, Germany

(Sigma-Aldrich), 2% FBS (StemCell Technologies, Vancouver, Canada), 1 × insulin-transferrin-selenium-X (ITS-X; Invitrogen), 1 × ALBU-Max I (Invitrogen), 1 × antibiotics-antimycotics (Invitrogen), 10 nM dexamethasone (Sigma-Aldrich), 50 μM ascorbic acid 2-phosphate (Sigma-Aldrich), 1 ng/mL epidermal growth factor (EGF; Peprotech, Rocky Hill, NJ, USA) and 10 ng/mL platelet-derived growth factor-BB (PDGF-BB; (R&D Systems, Minneapolis, MN, USA). After reaching 70–80% confluence, cells were replated at 20% confluence.

After cell expansion (passage 2), 70% confluent UCMS cells were differentiated into neuronal cells, adipocytes, osteocytes, chondrocytes, myoblasts, and pancreatic cells, as described previously (33–36). Briefly, prior to neuronal induction, UCMS cells were grown overnight in DMEM with 20% FBS (Invitrogen) and 10 ng/mL basic fibroblast growth factor (Peprotech). Cells were rinsed twice with PBS and incubated in DMEM with 100 μM butylated hydroxyanisole (BHA; Sigma-Aldrich), 10 μM forskolin (Sigma-Aldrich), 2% dimethyl sulfoxide (DMSO; Sigma-Aldrich), 5 U/mL heparin (Fuso Pharmaceutical Industries, Osaka, Japan), 5 nM K252a (Sigma-Aldrich), 25 mM KCl (Wako Pure Chemical Industries), 2 mM valproic acid (Sigma-Aldrich) and 1 × N2 supplement (Invitrogen). For differentiation into adipocytes, UCMS cells were incubated in DMEM with 1 μM dexamethasone, 0.5 mM 3-isobutyl-1-methlxanthine (Sigma-Aldrich), 1 μg/mL insulin (Sigma-Aldrich) and 100 μM indomethacin (Sigma-Aldrich). Differentiated cells were stained with Oil Red O (Sigma-Aldrich). For differentiation into osteocytes, UCMS cells were incubated in osteogenic differentiation medium in accordance with the manufacturer's protocol for 31 days (Invitrogen). Differentiated cells were stained with Alizarin Red S (Sigma-Aldrich). To investigate the potential formation of a chondrogenic pellet, UCMS cells were incubated in chondrogenic differentiation medium according to the manufacturer's protocol for 21 days (Invitrogen). Differentiated cell pellets were stained with Alcian Blue (Sigma-Aldrich) and cross-sections were studied. For differentiation into myoblasts, UCMS cells were initially incubated in DMEM with 2% FBS, 10 ng/mL EGF, 10 ng/mL PDGF-BB and 3 μM 5-azacytidine (Sigma-Aldrich) for 24 h. The medium was then changed to DMEM with 2% FBS, 10 ng/mL EGF and 10 ng/mL PDGF-BB. For differentiation into pancreatic cells, UCMS cells were cultured for 7 days in RPMI-1640 medium (Sigma-Aldrich) with 5% FBS and 10 mmol/L nicotinamide (Sigma-Aldrich). Cells were then cultured for an additional 5 days in the presence of 10 nM exendin 4 (Sigma-Aldrich).

Total RNA extraction and reverse transcriptase–polymerase chain reaction analysis

Total RNA was extracted from freshly isolated and *in vitro*-differentiated UCMS cells using RNeasy purification reagent (Qiagen, Hilden, Germany). Reverse transcriptase–polymerase chain reaction (RT-PCR) analysis was performed using a SuperScript One-Step RT-PCR System (Invitrogen) with 100 ng of tRNA. Sequences and annealing temperatures for each primer are described in Table II. The amplified cDNA was separated by electrophoresis through a 2% agarose gel, stained with ethidium bromide, and photographed under ultraviolet light.

GvHD model

Female B6C3F1 (recipient; C57BL/6 × C3H/He; H-$2^{b/k}$) and BDF1 (donor; C57BL/6 × DBA/2; H-$2^{b/d}$) mice between 8 and 12 weeks old were purchased from Japan SLC (Shizuoka, Japan). Mice were housed in sterile micro-isolator cages in a pathogen-free facility with *ad libitum* access to autoclaved food and hyperchlorinated drinking water. Donor bone marrow cells were harvested from tibiae and femurs by flushing with RPMI-1640 medium (Sigma-Aldrich). Recipient mice were lethally irradiated with 13 Gy total body irradiation (TBI; X-ray) split into two doses separated by 3 h. This amount of radiation and dose of infused donor cells has been shown to

Table II. Sequence of RT-PCR primers.

Gene	5′-primer	3′-primer	Temp. (°C)
Osteopontin	CTAGGCATCACCTGTGCCATACC	CAGTGACCAGTTCATCAGATTCATC	60
ALP	TCAGAAGCTCAACACCAACG	GTCAGGGACCTGGGCATT	51
Sox-9	ACATCTCCCCCAACGCCATC	TCGCTTCAGGTCAGCCTTGC	51
Aggrecan	TGCGGGTCAACAGTGCCTATC	CACGATGCCTTTCACCACGAC	51
PPARγ2	GCATTATGAGACATCCCCACTGC	CCTATTGACCCAGAAAGCGATTC	59
GFAP	CTGGGCTCAAGCAGTCTACC	AATTGCCTCCTCCTCCATCT	58
MAP-2	CTGCTTTACAGGGTAGCACAA	TTGAGTATGGCAAACGGTCTG	58
MyoD	GCTAGGTTCACGTTTCTCGC	GCGCCTTTATTTTGATCACC	58
Glucagon	GAGGGCTTGCTCTCTCTTCA	GTGAATGTGCCCTGTGAATG	57

ALP, alkaline phosphatase; GFAP, glial fibrillary acidic protein; MAP, microtubule-associated protein PPAR, peroxisome proliferator-activated receptor..

induce GvHD after hematopoietic stem cell transplantation (37). On the following day, donor-derived cells (1×10^7 bone marrow cells and 2×10^7 spleen cells) were suspended in 0.2 mL RPMI-1640 medium and transplanted via the tail vein into post-irradiation recipient mice. Soon after hematopoietic stem cell transplantation, 1×10^6 non-expanded and non-selected UCMS cells in 0.2 mL RPMI medium were transplanted via the tail vein. In the control group, the same amount of RPMI was infused via the tail vein. On day 7 after transplantation, the same number of non-expanded UCMS cells or RPMI medium alone was injected via the tail vein into treated mice or control mice, respectively. The severity of GvHD was evaluated using a scoring system incorporating five clinical parameters, as described previously (38): body weight; posture (hunching); mobility; fur texture; and skin integrity. Mice were evaluated and graded from 0 to 2 for each criterion. A clinical index was subsequently generated by summation of the five criteria scores (38). A score of 0–5 was defined as mild GvHD and a score of 6–10 or dead was defined as severe GvHD.

Statistical analysis

Statistical comparisons were performed using a Student's *t*-test or χ^2 test. For all experiments,

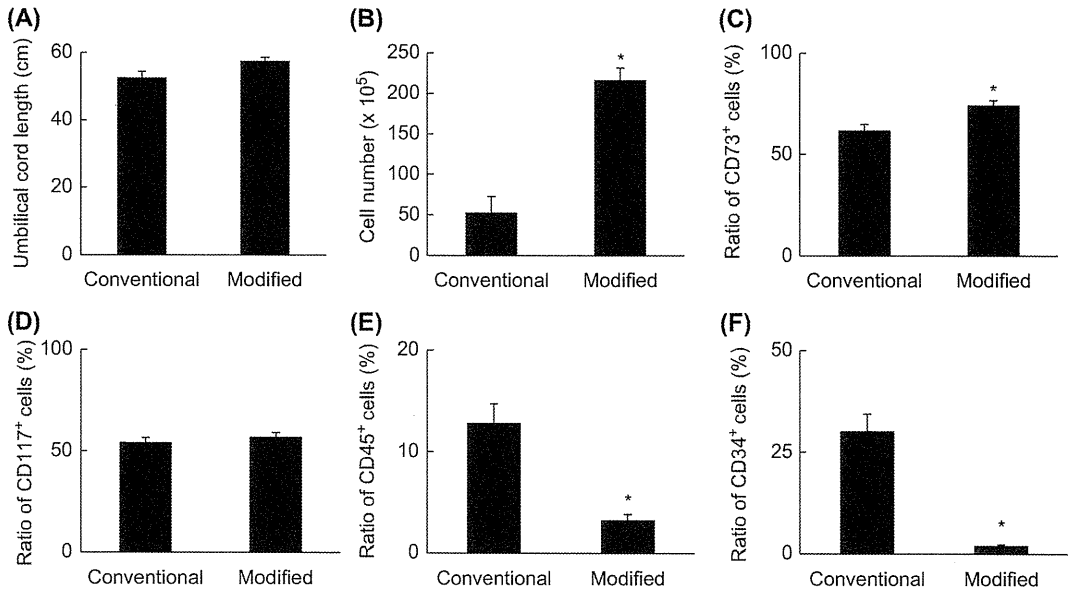

Figure 1. Cell numbers and characteristics of isolated MSC. No significant difference in the length of the umbilical cord was seen between groups (A). The total number of cells obtained with our modified method (216×10^5 cells) was more than 4-fold greater, compared with the conventional method (52×10^5 cells) (B). A significant increase in the ratio of cells expressing an MSC marker (CD73) was observed with the modified method (74.1%), compared with the conventional method (61.8%) (C). In contrast, no significant difference was observed in CD117-positive cells between modified (56.9%) and conventional methods (54.1%) (D). Contamination by cells from the hematopoietic lineage, expressing CD45 (E) and CD34 (F), was significantly decreased with the modified method (3.2% and 1.9%, respectively), compared with the conventional method (12.8% and 30.1%, respectively). $^*P < 0.05$ versus conventional method.

values are reported as mean ± standard error of the mean. Values of $P < 0.05$ were considered statistically significant.

Results

Characterization of isolated UCMS cells

MSC were isolated from umbilical cord using either conventional methods (29) ($n = 12$) or our modified methodology ($n = 18$). Although no significant differences in the length of umbilical cords were observed (Figure 1A), more than four times as many cells were obtained using our method (Figure 1B). To investigate the characteristics of these cells, surface cell markers were analyzed by flow cytometry for CD73, as an MSC marker (Figure 1C); a significant increase in the ratio of CD73-positive MSC was observed using our method, compared with the conventional technique. In contrast, no significant difference in the ratio of cells positive for the stem cell marker CD117 was identified between groups (Figure 1D). Umbilical cord contains a range of cell types, including hemocytes and endothelial cells. To investigate the level of these cells in our final cell population, numbers of CD45- and CD34-positive cells were investigated by flow cytometry (CD45, Figure 1E; CD34, Figure 1F). We observed a significant reduction in contamination by endothelial cells using our modified methodology compared with the conventional technique.

To evaluate properties of freshly isolated umbilical cord-derived cells, cell surface markers were analyzed by multiple staining for cell-surface markers. As shown in Figure 2, only a small fraction of CD73-positive cells displayed hemocyte/hematopoietic cell markers, including anti-CD11b, CD14, CD19, CD34, CD38, CD45, CD133, GlycophorinA and HLA-DR. These results indicated that the CD73-positive cell fraction contained a low level of hemocyte or hematopoietic cells. To evaluate the presence of endothelial cells in the CD73-positive cell fraction, the expression of various endothelial cell markers, including CD31, CD34 and von Willebrand Factor (vWF), was investigated; the majority of CD73-positive cells were negative for these endothelial cell markers. To confirm our results, expression of CD90, a marker not present on endothelial cells (39), was evaluated; more than 95% of CD73-positive cells expressed CD90. These findings indicated little contamination by endothelial cells using our modified methodology and were consistent with the visual impression that most vascular components remained undigested after incubation with hyaluronidase and collagenase for 2 h.

Changes in cell-surface markers of isolated umbilical cord-derived cells after in vitro expansion

To evaluate further the character of the isolated cell population, freshly prepared umbilical cord-derived cells using our modified methodology were cultured up to passage 4. Expanded cells showed a spindle-shaped morphology (Figure 3A) that associated with common MSC. Analysis of cell-surface markers revealed that expression of CD44 (Figure 3B; a cell-surface glycoprotein involved in cell–cell interactions expressed by mesenchymal cells), CD105 (Figure 3C; a membrane glycoprotein expressed

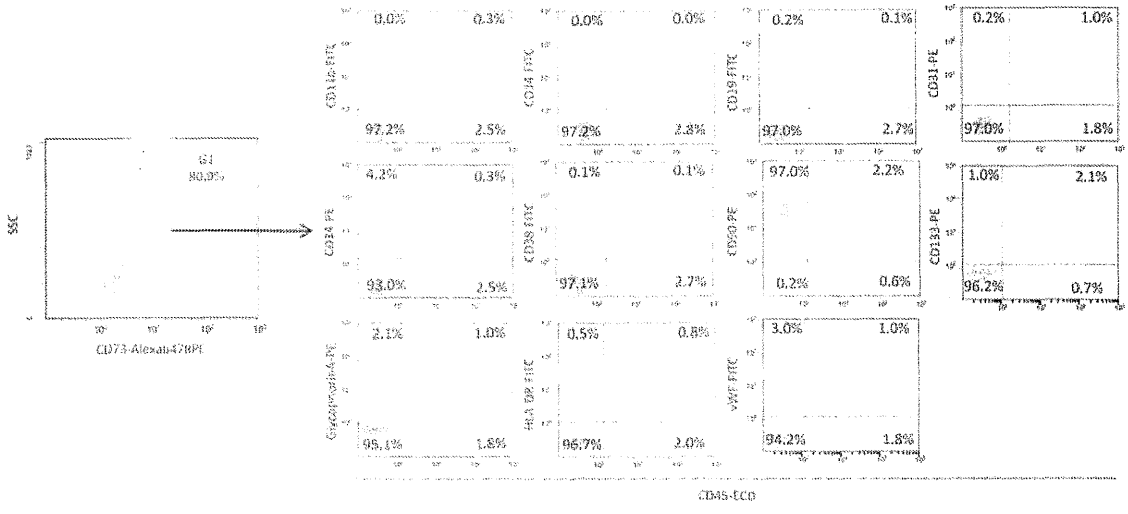

Figure 2. Multicolor analysis of freshly isolated MSC obtained by the modified protocol. To evaluate the presence of non-MSC, surface markers of freshly isolated cells were investigated. The majority of CD73-positive cells were negative for markers of hemocyte (CD11b, CD14, CD19, CD34, CD38, CD133, GlycophorinA, HLA-DR) and endothelial cell (CD31, vWF) lineages. It is notable that most of the CD73-positive cells expressed CD90, the latter not expressed on endothelial cells.

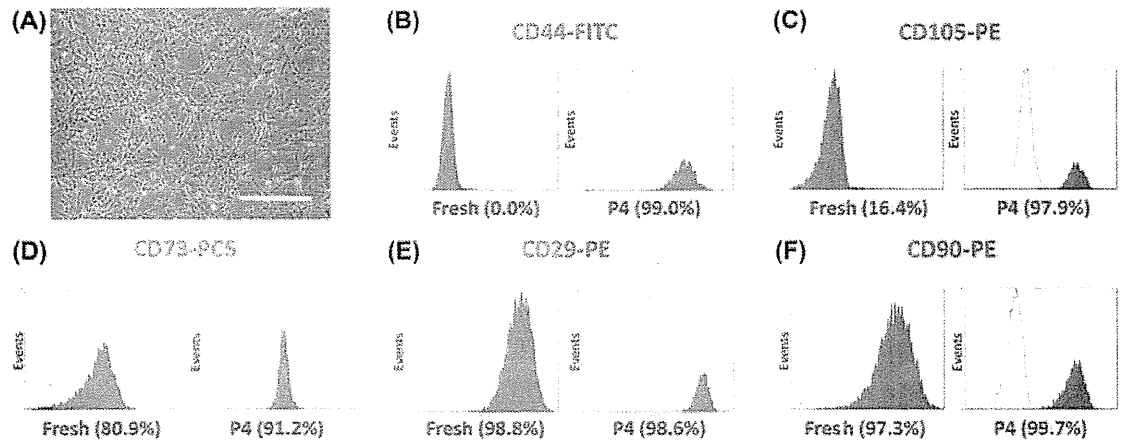

Figure 3. Changes in cell-surface markers associated with *in vitro* expansion. (A) Phase-contrast image of expanded UCMS cells. After *in vitro* expansion, analysis of MSC markers revealed an increased expression of CD44 (B), CD105 (C) and CD73 (D). In contrast, no change was observed in the expression of CD29 (E) and CD90 (F) because of *in vitro* expansion. Scale bar, 100 μm (A).

in multiple cell types including mesenchymal cells) and CD73 (Figure 3D; a nucleotidase expressed by multiple cells including mesenchymal cells) was increased in cells at passage 4. In contrast, expression of CD29 (Figure 3E; an integrin expressed in MSC) and CD90 (Figure 3F; a glycophosphatidylinositol-anchored cell-surface protein expressed by multiple cells including MSC) was similar to that observed prior to *ex vivo* expansion. These profiles were similar to amniotic-derived MSC as reported by De Coppi *et al.* (40).

Potential of UCMS cells

To investigate the potential of isolated UCMS cells to form differentiated cell types, the cell population was expanded under conditions conducive for osteocyte, chondrocyte or adipogenic differentiation. Under conditions conducive to the formation of osteocytes, on day 31 in cell culture Alizarin Red S-positive mineralized matrix-like nodules were observed (Figure 4A) and analysis of RNA confirmed the expression of osteocyte markers, osteopontin and alkaline phosphatase (ALP) (Figure 4B). Similarly, under conditions conducive to formation of a chondrogenic pellet, on day 21 in cell culture, Alcian Blue-positive chondrogenic-like pellets were observed (Figure 4C) and analysis of RNA confirmed the expression of chondrocyte markers, Sox-9 and aggrecan (Figure 4D). Under conditions leading to the formation of adipocytes, on day 20 of cell culture, Oil Red O-positive cells with lipid droplets were observed (Figure 4E, F) and analysis of RNA confirmed the expression of adipocyte marker peroxisome proliferator-activated receptor PPARγ2 (Figure 4G). Similarly, isolated cells incubated under conditions leading to neuronal differentiation showed subsequent expression of microtubule-associated protein 2 (MAP-2) and glial fibrillary acidic protein (GFAP) (Figure 4H). Furthermore, differentiated UCMS cells showed the myocyte marker MyoD (Figure 4I) and glucagon as a pancreatic cell marker (Figure 4J) when incubated under conditions leading to the formation of myocytes and pancreatic cells, respectively.

Suppression of GvHD by UCMS cells transplantation

In vitro-expanded MSC have been shown to suppress GvHD in patients after hematopoietic stem cell transplantation (41). To evaluate the potential for non-expanded UCMS cells to suppress GvHD, mice underwent allogeneic hematopoietic stem cell transplantation and were treated with non-expanded UCMS cells in RPMI. As a control, mice underwent allogeneic hematopoietic stem cell transplantation and were treated with RPMI alone. Mice were treated with non-expanded UCMS on days 0 and 6 after allogeneic stem cell transplantation, and the survival rate and severity of GvHD were investigated by 25 weeks after Bone Marrow Transplantation. (BMT). The frequency of severe GvHD at 6 weeks after allogeneic stem cell transplantation was significantly reduced with concomitant transplantation of non-expanded UCMS cells (Figure 4A). Although all mice in the control group showed severe GvHD or were already dead at 6 weeks, none of those treated with non-expanded UCMS cells (after the second treatment) were dead or showed severe GvHD. Representative pictures at 6 weeks in control and UCMS groups are shown in Figure 4B, C, respectively. Figure 4D shows the survival curve after allogeneic hematopoietic stem cell transplantation. Although no

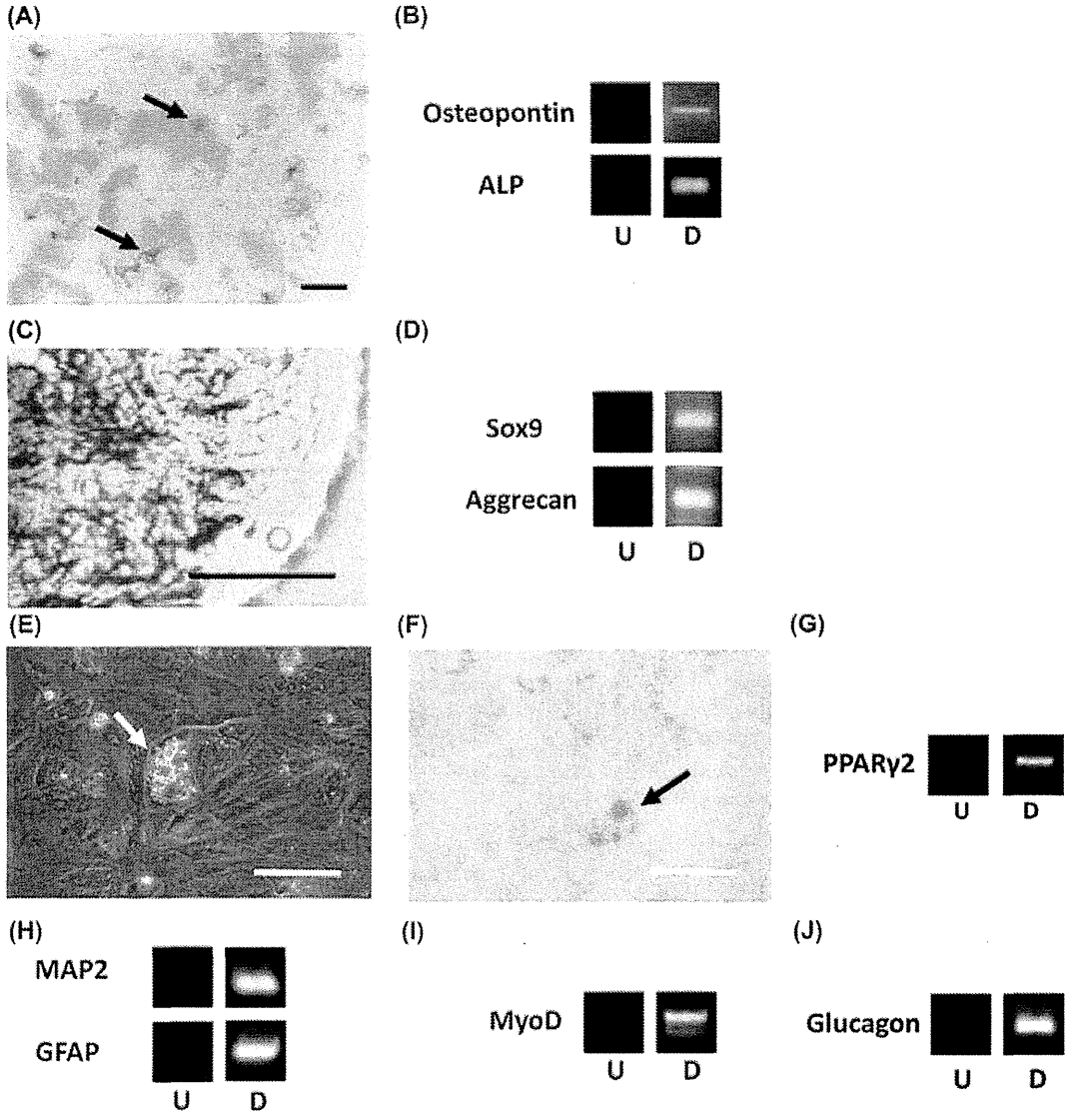

Figure 4. *In vitro* differentiation of freshly isolated UCMS cells. After expansion under conditions conducive to osteocyte or chondrocyte differentiation, Alizarin Red S-positive mineralized matrix-like nodules (A) or Alcian Blue-positive chondrogenic-like pellets (the latter displayed formation of layered structure at the surface) (C), respectively, were observed. UCMS cells cultured under conditions conductive to differentiation of osteocyte (B) and chondrocyte (D) cells expressed specific markers for each lineage. After expansion under conditions conducive to adipocyte differentiation, Oil Red O-positive adipocytes (E, phase-contrast image; F, Oil Red O staining) were observed and expression of PPARγ2 was observed (G). UCMS cells cultured under conditions conductive to differentiation of neuronal (H), myocyte (I) and pancreas (J) cells expressed specific markers for each lineage. Each experiment was repeated five times using different umbilical cord-derived cells. Scale bar, 40 μm (A), 100 μm (C, E, F). The arrow indicates Alizarin Red S-positive mineralized matrix-like nodules (A), lipid droplet (E) and Oil Red O-positive cells (F). U, undifferentiated; D, differentiated (B, D, G–J).

significant difference was apparent between groups at the 4-week assessment point, all of the mice in the control group were dead in 25 weeks, whereas no death was observed in mice with UCMS treatment group after the second treatment (Figure 5D).

Discussion

This study demonstrates that more than 2×10^7 MSC can be obtained safely from human umbilical cord without *in vitro* expansion and that these non-expanded MSC have the potential to suppress GvHD.

As a source of MSC, the umbilical cord has major advantages, including little contamination by cells of maternal origin, easy sterilization and few ethical problems. Compared with the method described by Weiss *et al.* (29), our modified method omits removal of blood vessels from the umbilical cord before treatment with collagenase and hyaluronidase.

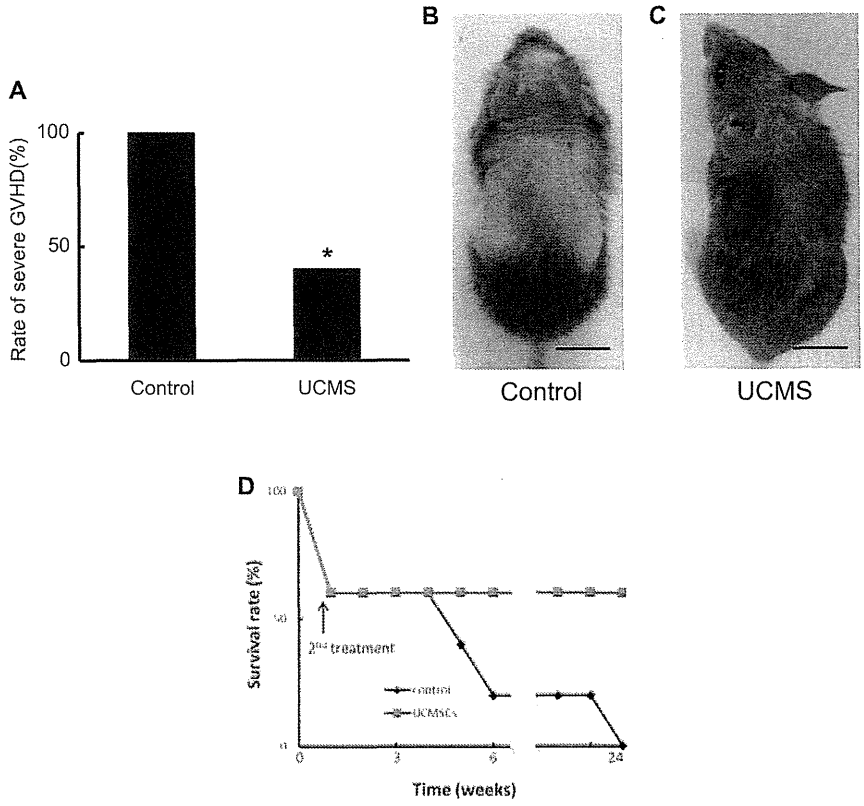

Figure 5. Suppression of GvHD by UCMS cells transplantation. Although all mice in the control group died or showed severe GvHD at 6 weeks (score 6; 1 mouse, dead; 4 mice), treatment with non-expanded UCMS cells significantly reduced the severity of GvHD (score 3; 1 mouse, score 4; 2 mice, dead; 2 mice) (A). Representative pictures of animals from the control group (B) and non-expanded UCMS cell-treated group (C) are shown. (D) Survival curve after radiation and allogeneic hematopoietic stem cell transplantation ($n = 5$, in each group). All of the mice in the control group were dead by 25 weeks after allogeneic hematopoietic stem cell transplantation. In contrast, no mice in the UCMS group were dead after the second infusion of non-expanded UCMS cells. $^*P < 0.05$ versus control. Scale bar, 1 cm (B, C).

Removal of the umbilical artery results in the loss of Wharton's jelly, which contains significant numbers of MSC. Preservation of the blood vessels before digestion with collagenase and hyaluronidase also significantly reduced contamination by endothelial cells. This finding may be attributed to removal of intact vascular structures from the cell suspension before digestion with trypsin, as vasculature was not considerably degraded in the presence of collagenase and hyaluronidase according to our protocol. Furthermore, our method has a significant advantage in that no *in vitro* cell culture is required for isolation of MSC from umbilical cord. In contrast, recently published methods described by Capelli *et al.* (11) and Lu *et al.* (10) involve cell culture over several days for isolation of MSC. The advantage of protocols using *in vitro* expansion is that non-adhesive cells can be removed, resulting in an enriched adhesive cell population. However, our results indicate that freshly isolated and non-selected umbilical cord-derived cells obtained by our method suppressed GvHD in an animal model. *In vitro* expansion of MSC carries a risk of tumorigenesis (42) and clinical use of the expanded cells requires strict monitoring to ensure safety. Our modified method has significant advantages in the reduced time required for the isolation procedure and its safety, both of which are important for cell banking. For the studies reported here, we used only the umbilical cords obtained at full-term Cesarean sections. It is likely that the properties and number of MSC in umbilical cord are similar comparing Cesarean section and vaginal delivery. Although caution should be taken regarding cleanliness/sterility after vaginal delivery, we expect that the same procedure can be used for umbilical cords obtained at full-term vaginal delivery.

In addition to offering a cell source for regenerative medicine, MSC have the potential to suppress GvHD after hematopoietic stem cell transplantation. Although the mechanisms and actual cell fraction underlying suppression of GvHD by MSC transplantation remains contentious (43), our results indicate

that human umbilical cord-derived non-expanded MSC suppressed GvHD in a murine model. The optimal type of MSC for suppression of GvHD, in terms of source, level of maturity and HLA-matching to the donor, is unclear. However, our results indicate that non-expanded UCMS cells represent a potential candidate cell source, particularly when co-banked with cord blood-derived hematopoietic cells (provided there is also strict control for contamination with infectious agents with HLA-typing). Furthermore, co-transplantation of HLA-matched hematopoietic stem cells and MSC may be advantageous to reduce clearance of transplanted MSC via immunologic recognition of HLA-matched hematopoietic cells.

In conclusion, our results indicate that umbilical cord-derived non-expanded MSC represent a potential cell source for cell banking and subsequent therapeutic use. Our results indicate that the combination of banking UCMS cells with identical cord blood-derived hematopoietic stem cells could be an important source for cell-based therapies in a range of settings.

Acknowledgments

This work was supported by a Grant-in-Aid for Scientific Research from the Ministry of Health, Labour and Welfare.

Declaration of interest: The authors declare no conflict of interest.

References

1. Liechty KW, MacKenzie TC, Shaaban AF, Radu A, Moseley AM, Deans R, et al. Human mesenchymal stem cells engraft and demonstrate site-specific differentiation after in utero transplantation in sheep. Nat Med. 2000;6:1282–6.
2. Schaffler A, Buchler C. Concise review. Adipose tissue-derived stromal cells: basic and clinical implications for novel cell-based therapies. Stem Cells. 2007;25:818–27.
3. Noth U, Osyczka AM, Tuli R, Hickok NJ, Danielson KG, Tuan RS. Multilineage mesenchymal differentiation potential of human trabecular bone-derived cells. J Orthop Res. 2002;20:1060–9.
4. De Bari C, Dell'Accio F, Luyten FP. Human periosteum-derived cells maintain phenotypic stability and chondrogenic potential throughout expansion regardless of donor age. Arthritis Rheum. 2001;44:85–95.
5. Hu Y, Liao L, Wang Q, Ma L, Ma G, Jiang X, et al. Isolation and identification of mesenchymal stem cells from human fetal pancreas. J Lab Clin Med. 2003;141:342–9.
6. in't Anker PS, Noort WA, Scherjon SA, Kleijburg-van der Keur C, Kruisselbrink AB, van Bezooijen RL, et al. Mesenchymal stem cells in human second-trimester bone marrow, liver, lung, and spleen exhibit a similar immunophenotype but a heterogeneous multilineage differentiation potential. Haematologica. 2003;88:845–52.
7. Huss R, Lange C, Weissinger EM, Kolb HJ, Thalmeier K. Evidence of peripheral blood-derived, plastic-adherent CD34(-/low) hematopoietic stem cell clones with mesenchymal stem cell characteristics. Stem Cells. 2000;18:252–60.
8. Rogers I, Casper RF. Umbilical cord blood stem cells. Best Pract Res Clin Obstet Gynaecol. 2004;18:893–908.
9. Romanov YA, Svintsitskaya VA, Smirnov VN. Searching for alternative sources of postnatal human mesenchymal stem cells: candidate MSC-like cells from umbilical cord. Stem Cells. 2003;21:105–10.
10. Lu LL, Liu YJ, Yang SG, Zhao QJ, Wang X, Gong W, et al. Isolation and characterization of human umbilical cord mesenchymal stem cells with hematopoiesis-supportive function and other potentials. Haematologica. 2006;91:1017–26.
11. Capelli C, Gotti E, Morigi M, Rota C, Weng L, Dazzi F, et al. Minimally manipulated whole human umbilical cord is a rich source of clinical-grade human mesenchymal stromal cells expanded in human platelet lysate. Cytotherapy. 2011;13:786–801.
12. Bjorklund A, Lindvall O. Cell replacement therapies for central nervous system disorders. Nat Neurosci. 2000;3: 537–44.
13. Galle J, Bader A, Hepp P, Grill W, Fuchs B, Kas JA, et al. Mesenchymal stem cells in cartilage repair: state of the art and methods to monitor cell growth, differentiation and cartilage regeneration. Curr Med Chem. 2010;17:2274–91.
14. Liu H, Zhang J, Liu CY, Wang IJ, Sieber M, Chang J, et al. Cell therapy of congenital corneal diseases with umbilical mesenchymal stem cells: lumican null mice. PLoS One. 2010;5:1–4.
15. Lee JS, Hong JM, Moon GJ, Lee PH, Ahn YH, Bang OY. A long-term follow-up study of intravenous autologous mesenchymal stem cell transplantation in patients with ischemic stroke. Stem Cells. 2010;28:1099–106.
16. Schuleri KH, Feigenbaum GS, Centola M, Weiss ES, Zimmet JM, Turney J, et al. Autologous mesenchymal stem cells produce reverse remodelling in chronic ischaemic cardiomyopathy. Eur Heart J. 2009;30:2722–32.
17. Lim JH, Lee MH, Yi HG, Kim CS, Kim JH, Song SU. Mesenchymal stromal cells for steroid-refractory acute graft-versus-host disease: a report of two cases. Int J Hematol. 2010;92:204–7.
18. Portmann-Lanz CB, Schoeberlein A, Huber A, Sager R, Malek A, Holzgreve W, et al. Placental mesenchymal stem cells as potential autologous graft for pre- and perinatal neuroregeneration. Am J Obstet Gynecol. 2006;194:664–73.
19. in't Anker PS, Scherjon SA, Kleijburg-van der Keur C, Noort WA, Claas FH, Willemze R, et al. Amniotic fluid as a novel source of mesenchymal stem cells for therapeutic transplantation. Blood. 2003;102:1548–9.
20. Erices A, Conget P, Minguell JJ. Mesenchymal progenitor cells in human umbilical cord blood. Br J Haematol. 2000;109:235–42.
21. Wang HS, Hung SC, Peng ST, Huang CC, Wei HM, Guo YJ, et al. Mesenchymal stem cells in the Wharton's jelly of the human umbilical cord. Stem Cells. 2004;22:1330–7.
22. Meyer FA, Laver-Rudich Z, Tanenbaum R. Evidence for a mechanical coupling of glycoprotein microfibrils with collagen fibrils in Wharton's jelly. Biochim Biophys Acta. 1983;755:376–87.
23. McElreavey KD, Irvine AI, Ennis KT, McLean WH. Isolation, culture and characterisation of fibroblast-like cells derived from the Wharton's jelly portion of human umbilical cord. Biochem Soc Trans. 1991;19:29S.
24. Covas DT, Siufi JL, Silva AR, Orellana MD. Isolation and culture of umbilical vein mesenchymal stem cells. Braz J Med Biol Res. 2003;36:1179–83.

25. Sarugaser R, Lickorish D, Baksh D, Hosseini MM, Davies JE. Human umbilical cord perivascular (HUCPV) cells: a source of mesenchymal progenitors. Stem Cells. 2005;23:220–9.
26. Fu YS, Shih YT, Cheng YC, Min MY. Transformation of human umbilical mesenchymal cells into neurons in vitro. J Biomed Sci. 2004;11:652–60.
27. Fu YS, Cheng YC, Lin MY, Cheng H, Chu PM, Chou SC, et al. Conversion of human umbilical cord mesenchymal stem cells in Wharton's jelly to dopaminergic neurons in vitro: potential therapeutic application for Parkinsonism. Stem Cells. 2006;24:115–24.
28. Kadivar M, Khatami S, Mortazavi Y, Shokrgozar MA, Taghikhani M, Soleimani M. In vitro cardiomyogenic potential of human umbilical vein-derived mesenchymal stem cells. Biochem Biophys Res Commun. 2006;340:639–47.
29. Weiss ML, Medicetty S, Bledsoe AR, Rachakatla RS, Choi M, Merchav S, et al. Human umbilical cord matrix stem cells: preliminary characterization and effect of transplantation in a rodent model of Parkinson's disease. Stem Cells. 2006;24: 781–92.
30. Chao KC, Chao KF, Fu YS, Liu SH. Islet-like clusters derived from mesenchymal stem cells in Wharton's jelly of the human umbilical cord for transplantation to control type 1 diabetes. PLoS One. 2008;3:1–9.
31. Carlin R, Davis D, Weiss M, Schultz B, Troyer D. Expression of early transcription factors Oct-4, Sox-2 and Nanog by porcine umbilical cord (PUC) matrix cells. Reprod Biol Endocrinol. 2006;4:1–13.
32. Rubinstein P, Dobrila L, Rosenfield RE, Adamson JW, Migliaccio G, Migliaccio AR, et al. Processing and cryopreservation of placental/umbilical cord blood for unrelated bone marrow reconstitution. Proc Natl Acad Sci USA. 1995;92:10119–22.
33. Woodbury D, Reynolds K, Black IB. Adult bone marrow stromal stem cells express germline, ectodermal, endodermal, and mesodermal genes prior to neurogenesis. J Neurosci Res. 2002;69:908–17.
34. Dennis JE, Merriam A, Awadallah A, Yoo JU, Johnstone B, Caplan AI. A quadripotential mesenchymal progenitor cell isolated from the marrow of an adult mouse. J Bone Miner Res. 1999;14:700–9.
35. Reyes M, Lund T, Lenvik T, Aguiar D, Koodie L, Verfaillie CM. Purification and ex vivo expansion of postnatal human marrow mesodermal progenitor cells. Blood. 2001;98:2615–25.
36. Tang DQ, Cao LZ, Burkhardt BR, Xia CQ, Litherland SA, Atkinson MA, et al. In vivo and in vitro characterization of insulin-producing cells obtained from murine bone marrow. Diabetes. 2004;53:1721–32.
37. Taniguchi Y, Yoshihara S, Hoshida Y, Inoue T, Fujioka T, Ikegame K, et al. Recovery from established graft-vs-host disease achieved by bone marrow transplantation from a third-party allogeneic donor. Exp Hematol. 2008;36:1216–25.
38. Cooke KR, Kobzik L, Martin TR, Brewer J, Delmonte J Jr, Crawford JM, et al. An experimental model of idiopathic pneumonia syndrome after bone marrow transplantation. I. The roles of minor H antigens and endotoxin. Blood. 1996;88:3230–9.
39. Mutin M, Dignat-George F, Sampol J. Immunologic phenotype of cultured endothelial cells: quantitative analysis of cell surface molecules. Tissue Antigens. 1997;50:449–58
40. De Coppi P, Bartsch G Jr, Siddiqui MM, Xu T, Santos CC, Perin L, et al. Isolation of amniotic stem cell lines with potential for therapy. Nat Biotechnol. 2007;25:100–6.
41. Le Blanc K, Frassoni F, Ball L, Locatelli F, Roelofs H, Lewis I, et al. Mesenchymal stem cells for treatment of steroid-resistant, severe, acute graft-versus-host disease: a phase II study. Lancet. 2008;371:1579–86.
42. Spaeth EL, Dembinski JL, Sasser AK, Watson K, Klopp A, Hall B, et al. Mesenchymal stem cell transition to tumor-associated fibroblasts contributes to fibrovascular network expansion and tumor progression. PLoS One. 2009; 4:1–11.
43. Sato K, Ozaki K, Mori M, Muroi K, Ozawa K. Mesenchymal stromal cells for graft-versus-host disease : basic aspects and clinical outcomes. J Clin Exp Hematop. 2010;50:79–89.

Neurochemistry International 61 (2012) 240–250

Contents lists available at SciVerse ScienceDirect

Neurochemistry International

journal homepage: www.elsevier.com/locate/nci

Linkage of N-cadherin to multiple cytoskeletal elements revealed by a proteomic approach in hippocampal neurons

Hidekazu Tanaka [a,*], Kazuaki Takafuji [a], Akihiko Taguchi [b], Pattama Wiriyasermkul [a], Ryuichi Ohgaki [a], Shushi Nagamori [a], Pann-Ghill Suh [c], Yoshikatsu Kanai [a]

[a] Department of Pharmacology, Osaka University School of Medicine, Osaka 565-0871, Japan
[b] Institute of Biomedical Research and Innovation, Kobe 650-0047, Japan
[c] Advanced Research Center for Signal Transduction in Cancers, Ulsan National Institute of Science and Technology, Ulsan 689-798, Republic of Korea

ARTICLE INFO

Article history:
Received 5 April 2012
Received in revised form 7 May 2012
Accepted 9 May 2012
Available online 17 May 2012

Keywords:
Synapse
Plasticity
Adhesion
Cadherin
Cytoskeleton
Hippocampus

ABSTRACT

The CNS synapse is an adhesive junction differentiated for chemical neurotransmission and is equipped with presynaptic vesicles and postsynaptic neurotransmitter receptors. Cell adhesion molecule cadherins not only maintain connections between pre- and postsynaptic membranes but also modulate the efficacy of synaptic transmission. Although the components of the cadherin-mediated adhesive apparatus have been studied extensively in various cell systems, the complete picture of these components, particularly at the synaptic junction, remains elusive. Here, we describe the proteomic assortment of the N-cadherin-mediated synaptic adhesion apparatus in cultured hippocampal neurons. N-cadherin immunoprecipitated from Triton X-100-solubilized neuronal extract contained equal amounts of β- and α-catenins, as well as F-actin-related membrane anchor proteins such as integrins bridged with α-actinin-4, and Na^+/K^+-ATPase bridged with spectrins. A close relative of β-catenin, plakoglobin, and its binding partner, desmoplakin, were also found, suggesting that a subset of the N-cadherin-mediated adhesive apparatus also anchors intermediate filaments. Moreover, dynein heavy chain and LEK1/CENPF/mitosin were found. This suggests that internalized pools of N-cadherin in trafficking vesicles are conveyed by dynein motors on microtubules. In addition, ARVCF and NPRAP/neurojungin/δ2-catenin, but not p120ctn/δ1-catenin or plakophilins-1, -2, -3, -4 (p0071), were found, suggesting other possible bridges to microtubules. Finally, synaptic stimulation by membrane depolarization resulted in an increased 93-kDa band, which corresponded to proteolytically truncated β-catenin. The integration of three different classes of cytoskeletal systems found in the synaptic N-cadherin complex may imply a dynamic switching of adhesive scaffolds in response to synaptic activity.

1. Introduction

The CNS synapse is an adhesive junction differentiated for chemical transmission and is equipped with presynaptic vesicles and postsynaptic neurotransmitter receptors. Cell adhesion molecules that link pre- and postsynaptic membranes not only maintain specific synaptic connections but also regulate the efficacy of synaptic transmission and plasticity (Bozdagi et al., 2004; Jungling et al., 2006; Okamura et al., 2004; Tanaka et al., 2000). Proteins assembled for the cadherin-mediated adherens junction have been extensively studied in various cell systems. However, different cadherins have been studied in distinct cell system models. Hence, it is unclear which proteins are genuinely assembled in synaptic junctions.

Cadherins are large superfamily of transmembrane cell adhesion proteins with characteristic extracellular repeats of about 110 amino acids. The cadherin superfamily comprises the classic cadherin and protocadherin subfamilies. Classic cadherins share conserved cytoplasmic domains that bind to β-catenin, whereas protocadherins have diversiform cytoplasmic domains connected to a wide variety of intracellular signaling molecules (Yagi and Takeichi, 2000). Classic cadherins are expressed in synaptic junctions (Benson and Tanaka, 1998; Fannon and Colman, 1996; Manabe et al., 2000; Uchida et al., 1996). Among them, N-cadherin

Abbreviations: AMPA, 2-amino-3-(5-methyl-3-oxo-1,2-oxazol-4-yl)propanoic acid; CNS, central nervous system; HBSS, Hanks' balanced salt solution; LC–MS/MS, liquid chromatography–tandem mass spectrometry; MAP kinase, mitogen-activated protein kinase; MT, microtubule; NMDA, *N*-methyl-D-aspartate; PAGE, polyacrylamide gel electrophoresis; PPW, presynaptic particle web; PSD, postsynaptic density; SDS, sodium dodecyl sulfate.

* Corresponding author. Address: Department of Pharmacology A6, Osaka University School of Medicine, 2-2 Yamadaoka, Suita, Osaka 565-0871, Japan. Tel.: +81 6 6879 3521; fax: +81 6 6879 3529.
E-mail address: htanaka@pharma1.med.osaka-u.ac.jp (H. Tanaka).

0197-0186/$ - see front matter © 2012 Elsevier Ltd. All rights reserved.
http://dx.doi.org/10.1016/j.neuint.2012.05.008

has been intensively investigated in hippocampal neurons and has been proven to play various roles in synaptic transmission and plasticity (Bozdagi et al., 2000; Jungling et al., 2006; Tang et al., 1998). The involvement of N-cadherin in synaptic activity is also supported by studies on cadherin-interacting proteins such as β-catenin (Okuda et al., 2007), δ-catenin (Israely et al., 2004), and IQ-GAP/ERK (Schrick et al., 2007).

Accumulating evidence indicates the involvement of N-cadherin as a dynamic feature of synaptic physiology. For example, N-cadherin mediates an activity-induced enlargement of the dendritic spine, which is dependent on rearrangement of the actin cytoskeleton (Okamura et al., 2004). Concomitantly, N-cadherin can undergo conformational change, e.g. dimerization, with acquired resistance to trypsin (Tanaka et al., 2000). At the same time, N-cadherin shows enhanced binding to β-catenin (Murase et al., 2002) and stabilization on the cell surface (Tai et al., 2007). The immobilization of N-cadherin/β-catenin parallels with the stabilization of actin filaments by synaptic stimulation (Fischer et al., 2000; Fukazawa et al., 2003; Lin et al., 2005; Okamoto et al., 2004; Star et al., 2002). There are also suggestions that the N-cadherin–catenin complex is more directly linked to presynaptic vesicular physiology (Bamji et al., 2003, 2006; Bozdagi et al., 2004; Jungling et al., 2006) as well as postsynaptic neurotransmitter receptors (Saglietti et al., 2007). Furthermore, there are pathways that force N-cadherin into intracellular compartments. One pathway involves steady-state endocytosis, which is inhibited by the activation of the NMDA receptor (Tai et al., 2007). Another is an activity-regulated endocytic pathway, in which arcadlin (protocadherin-8), induces endocytosis of N-cadherin as a downstream event of p38 MAP kinase activation (Yasuda et al., 2007).

Thus, N-cadherin plays multiple, dynamic roles in synaptic remodeling and plasticity. Synaptic N-cadherin should therefore be linked to distinct cellular mechanisms that are specialized for separate, specific tasks. Here, we focus on the rodent hippocampal synapse to directly depict the cadherin-mediated adhesion complex. We describe the proteomic assortment of the synaptic adhesion apparatus assisted by N-cadherin in cultured hippocampal neurons. The protein complexes assembled with N-cadherin were consistent with the N-cadherin linkages to F-actins, intermediate filaments, and microtubules. In addition, synaptic stimulation by membrane depolarization resulted in the increase of a 93-kDa band, which corresponded to proteolytically truncated β-catenin. The integration of three different cytoskeletal systems takes place in N-cadherin-mediated adhesive machinery, providing a dynamic scaffold underlying synaptic plasticity.

2. Materials and methods

2.1. Neuron culture

Hippocampal neurons were cultured from E18 rat embryos as previously described (Tanaka et al., 2000). Neurons were plated at a density of 1.4–2.1 × 10^4 cells/cm^2 onto poly-L-lysine-coated dishes (Φ = 35 mm). Neurons were maintained in Neurobasal medium supplemented with B27 (Life Technologies) and 5 μM cytosine arabinoside.

2.2. Protein extraction, immunoprecipitation, and immunoblotting

Hippocampi were dissected from adult C57BL/6 mice, homogenized in Ca-PI-lysis buffer (10 mM HEPES–NaOH (pH 7.4), 1% Triton X-100, 120 mM NaCl, 2 mM $CaCl_2$, 10 μg/ml leupeptin, 10 μg/ml pepstatin A, 1 μg/ml aprotinin, 0.2 mM phenylmethylsulfonyl fluoride, 20 mM NaF, 20 mM β-glycerophosphate, and 1 mM Na_3VO_4) with a Teflon-glass homogenizer, and centrifuged for 1 h to obtain clear protein extracts. Mature neurons cultured for 4–5 weeks were depolarized with 50 mM KCl for 15 min. Neurons were washed twice with chilled PBS, harvested with 80 μl (for a Φ = 35 mm dish) of Ca-PI-lysis buffer, sonicated, and centrifuged. N-cadherin-associated protein complex was immunoprecipitated from these samples with 0.5–2.5 μg of murine anti-N-cadherin (BD Transduction Laboratories). The precipitated protein complex was separated in 4–15% gradient SDS–PAGE followed by either silver staining, Sypro Ruby (Molecular Probes) staining, or immunoblotting. Immunoblots were probed with murine anti-α-catenin (BD Transduction Laboratories, 1:5000), murine anti-p120 (BD Transduction Laboratories, 1:2500), murine anti-plakoglobin (BD Transduction Laboratories, 1:2000), rabbit anti-syntaxin 1 (Sigma–Aldrich, 1:10000), rabbit anti-JLP (SPAG9) (Abcam, 1:10000), rabbit anti-pan-14-3-3 (Millipore, 1:5000), murine anti-TRAP1 (BD Transduction Laboratories 1:5000), rabbit anti-DDB1 (Abcam, 1:5000), and rabbit anti-TRIM33 (Bethyl Laboratories, 1:2000) antibodies.

2.3. Sequential extraction of synaptosome fractions

Hippocampi isolated from two mice were homogenized (Dounce homogenizer, 30 strokes) in buffered sucrose (0.32 M sucrose in hypotonic A buffer). Hypotonic A buffer contained 4 mM HEPES–NaOH (pH 7.4), 1 mM $MgCl_2$, 0.5 mM $CaCl_2$, and 0.0025% butylated hydroxy toluene. The homogenate was centrifuged (800g × 10 min) and the supernatant (S1) was centrifuged again (9200g × 15 min) to collect the precipitate (P2). The P2 pellet was resuspended in buffered sucrose and overlaid on stepwise sucrose gradients (0.85, 1.0, and 1.2 M) and ultracentrifuged at 82,500g for 120 min. The crude synaptosome fraction accumulated between 1.0 and 1.2 M cushions was collected, diluted with 3 × volume of hypotonic A buffer, and ultracentrifuged (32,800g × 20 min). The resultant synaptosome pellet was resuspended in 120 μl of isotonic buffer B (10 mM HEPES–NaOH (pH 7.4), 120 mM NaCl, 1 mM $MgCl_2$, 0.5 mM $CaCl_2$, 0.0025% butylated hydroxy toluene, 10 μg/ml leupeptin, 10 μg/ml pepstatin A, 1 μg/ml aprotinin, and 0.2 mM phenylmethylsulfonyl fluoride), mixed with 30 μl of 0.1 M methyl-β-cyclodextrin, and incubated at 37 °C for 15 min followed by centrifugation (15,000 rpm × 15 min at 23 °C). After removing the supernatant as a methyl-β-cyclodextrin extract, the pellet was resuspended in 150 μl of stripping buffer (5 M urea dissolved in isotonic buffer B) and centrifuged as previously to obtain a urea extract and stripped-membrane pellet. The urea-stripped membrane pellet was resuspended in 150 μl of solubilizing buffer (1% Triton X-100 dissolved in isotonic buffer B) and centrifuged to obtain a Triton extract and an insoluble pellet.

2.4. In-gel digestion

Gel pieces were excised from Sypro Ruby-stained gels and washed with 50% (v/v) acetonitrile and 50 mM NH_4HCO_3, pH 8.0, for 30 min to remove the fluorescence dye. Gel pieces were then soaked in acetonitrile for 5 min, acetonitrile was removed, and the gel pieces were dried for 20 min in a vacuum. Prior to enzymatic digestion, gel pieces were reduced with 10 mM dithiothreitol in 50 mM NH_4HCO_3 at 37 °C for 30 min, then alkylated with 55 mM iodoacetamide in 50 mM NH_4HCO_3 for 30 min, and dehydrated by addition of acetonitrile. The reduced and alkylated gel pieces were rehydrated in 50 mM Tris–HCl, pH 9.0, and 0.5 μg/ml sequencing grade modified trypsin (Roche Diagnostics). Once this solution was fully absorbed by the gel pieces, enzyme-free Tris–HCl buffer was added until the gel pieces were covered. The samples were digested for 16 h at 37 °C, extracted with acetonitrile and 5% formic acid for 20 min, and acetonitrile was evaporated using a Speed-Vac centrifuge. The tryptic digests were desalted

with C18-StageTips, concentrated using the Speed-Vac centrifuge, and reconstituted in 0.1% formic acid and 3% acetonitrile.

2.5. In-solution digestion for shotgun analyses

Immunoprecipitated samples were added to 50 mM Tris–HCl, pH 9.0, reduced with 10 mM dithiothreitol at 37 °C for 30 min, alkylated with 55 mM iodoacetamide in the dark at room temperature for 30 min, and digested with 0.5 μg/ml sequencing grade modified trypsin at 37 °C for 16 h. The digests were desalted and reconstituted as above.

2.6. LC–MS/MS and data analysis

LC–MS/MS analysis was performed by a Paradigm MS4 nano-HPLC system (Michrom BioResources, Inc., Auburn, CA) coupled to an LTQ linear ion trap mass spectrometer (Thermo Electron Corp., Waltham, MA) with a nanoelectrospray ionization source (AMR Inc., Tokyo, Japan). Tryptic peptides were injected by an HTC-PAL autosampler (CTC Analytics AG, Zwingen, Switzerland) and enriched on a C18 trap column (300 μm I.D. × 5 mm length, CERI, Tokyo, Japan) at a flow rate of 6 μl/min. The samples were subsequently separated by a C18 reverse phase column (100 μm I.D. × 150 mm length, Nikkyo Technos Co., Ltd., Tokyo, Japan) at a flow rate of 1 μl/min with a linear gradient from 2% to 65% mobile phase B, i.e. from 98% to 35% of mobile phase A. Mobile phase B consisted of 95% acetonitrile with 0.1% formic acid, whereas mobile phase A consisted of 2% acetonitrile with 0.1% formic acid. LC–MS/MS analysis was carried out using data-dependent triple-play mode. Automated gain control values were set at 1.5×10^4, 1.5×10^3, and 5.0×10^3 for Full-MS, Zoom-MS, and MS/MS, respectively. A spray voltage of 1.6 kV was applied. The MS scan range was m/z 300–2000. Peptides and proteins were identified by Mascot v2.2 (Matrix Science, London, UK) with a maximum tolerance of 1.2 Da for MS data, 0.5 Da for MS/MS data, and strict trypsin specificity allowing for up to one missed cleavage. Carbamidomethylation of cysteine and oxidation of methionine were allowed as a variable modification.

2.7. Trypsin treatment of living neurons

Modification of N-cadherin in response to synaptic stimulation was demonstrated by the acquired resistance to trypsin as reported (Tanaka et al., 2000). Stimulated and control neurons, maintained in 35 mm dishes (14,400 cells/cm^2), were washed briefly with prewarmed (37 °C) HEPES-buffered (10 mM, pH 7.4) HBSS and covered with 0.1% trypsin (Life Technologies) diluted with HBSS. The excess trypsin solution was removed immediately, followed by incubation for 10 min at 37 °C. The digested neurons were directly harvested in SDS–PAGE sample buffer (80 μl), or 40 μl of Ca-lysis buffer supplemented with soybean trypsin inhibitor (10 mM HEPES–NaOH (pH 7.4), 1% Triton X-100, 120 mM NaCl, 2 mM $CaCl_2$, 10 μg/ml leupeptin, 10 μg/ml pepstatin A, 1 μg/ml aprotinin, 0.2 mM phenylmethylsulfonyl fluoride, and 0.01% trypsin inhibitor) followed by centrifugation (15,000 rpm × 5 min at 4 °C) to obtain the Triton-soluble supernatant and the Triton-insoluble pellet. The supernatant was mixed with 5 × SDS–PAGE sample buffer (10 μl), and the pellet was resuspended in SDS–PAGE sample buffer containing 4 M urea (40 μl).

3. Results and discussion

3.1. Strategy

N-cadherin is expressed in synaptic membranes of hippocampal neurons (Benson and Tanaka, 1998; Tanaka et al., 2000). Synaptic N-cadherin appears to comprise: a surface pool in the endocytic zone located in the periphery of the synapse (Tanaka et al., 2000; Uchida et al., 1996), an intracellular pool such as endosomes (Tai et al., 2007; Yasuda et al., 2007), and an active zone pool associated with the presynaptic particle web (PPW) and postsynaptic density (PSD) (Fig. 1A) (Phillips et al., 2001).

The active zone-associated electron-dense structures (PPW + PSD), which correspond to so-called synaptic junctions, are biochemically characterized by the insolubility in 1% Triton X-100 (Phillips et al., 2001). Approximately 60% of N-cadherin was collected in the Triton-soluble fraction and 40% in the Triton-insoluble fraction (Fig. 1B,C). In the epithelial cells, the Triton-insoluble fraction is comprised of cytoskeleton-associated scaffolding protein complexes and cholesterol-rich lipid rafts (Brown and Rose, 1992). N-cadherin was not extracted from the crude synaptosome fraction with methyl-β-cyclodextrin, a cholesterol-extracting agent, suggesting that the Triton-insoluble N-cadherin is largely integrated into the synaptic junctional complex (Fig. 1B,C). Usually, biochemical analyses of the synaptic junctions utilize these Triton-insoluble PSD fractions (Cotman et al., 1974). For example, in immunoprecipitation experiments, the PSD is solubilized with high concentration of ionic detergent (e.g., 10% sodium deoxycholate), and then the detergent is diluted, so that the disrupted proteins may reassemble, allowing the reassembled protein complexes to be co-immunoprecipitated (Luo et al., 1997).

The surface endocytic zone and endosome pools of N-cadherin (Fig. 1A (1) and (2)) are also supposed to be involved in the plasticity of synaptic structures, and are largely soluble in 1% Triton X-100 by several reasons. First, the surface pools undergo vigorous redistributions by synaptic acitivity (Okamura et al., 2004; Tanaka et al., 2000). These mobile pools were extractable with 1% Triton X-100 in our unpublished observations. Second, the endocytosed N-cadherin is shown to be extracted with 1% Triton X-100/0.1% SDS as detected in western blotting (Tai et al., 2007). Third, the synaptic stimulation-induced trypsin-resistance of N-cadherin was readily detectable in the Triton-soluble fraction as well as in the Triton-insoluble fraction (Fig. 1D). The acquired trypsin-resistance of N-cadherin is a sign of conformational change in response to synaptic activity, and this implies rearrangements of protein–protein interactions (Tanaka et al., 2000).

Thus we reasoned that the determination of protein–protein interactions within the Triton-soluble fraction from synapse-enriched neuronal lysate provides insight into the mechanisms involved in the dynamism of the synaptic structure. There are several advantages by focusing on the Triton-soluble fraction. First, we are able to avoid artificial disruption/reassembly of protein complexes with ionic detergent and its dilution. The intrinsic interactions are directly captured by one-step lysis with Triton X-100. Second, Triton X-100 is a non-ionic detergent and expected to maintain relatively weak protein–protein interactions. The expected disadvantage is that this approach fails to detect the strong protein–protein interactions that involve scaffolding proteins within the PSD.

We used rat hippocampal neurons cultured for 5–6 weeks. Neurons at this stage develop enormous numbers of mature synaptic junctions that are positive for N-cadherin with little contamination by glial cells (Tanaka et al., 2000). Most N-cadherin-positive synaptic puncta cluster at PSD-95-containing postsynaptic densities, a marker of excitatory synapses, but not at GABAergic termini (Benson and Tanaka, 1998). After solubilizing the neurons with 1% Triton X-100, N-cadherin was immunoprecipitated and subjected to SDS–PAGE (Fig. 2A). The bands in the gel specific for anti-N-cadherin antibody but not for control IgG were excised and subjected to in-gel digestion followed by LC–MS/MS analysis (Fig. 2B, Table 1).

We also performed shotgun LC–MS/MS analysis of murine hippocampal extracts in the same buffer conditions. In these

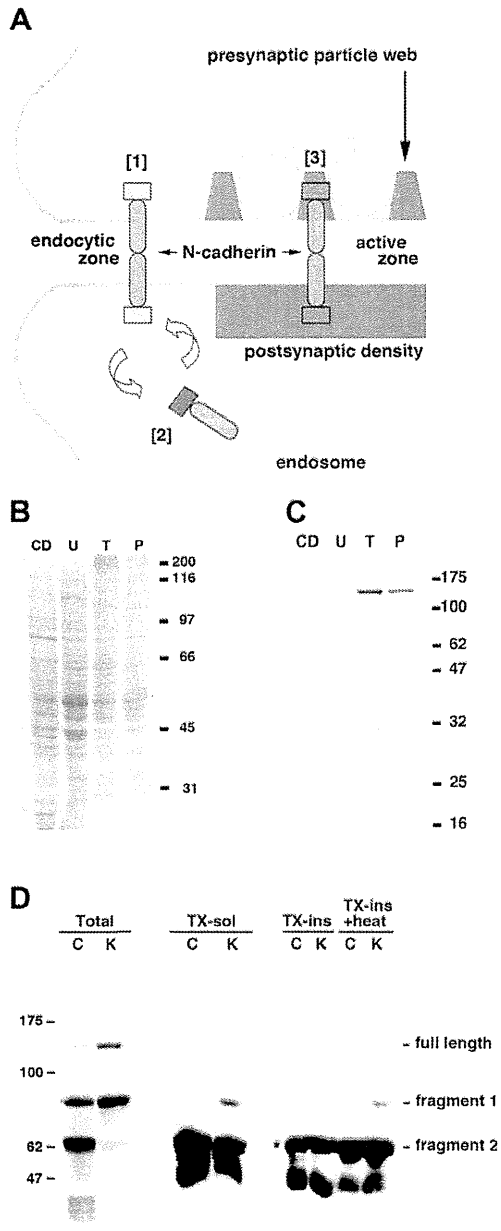

Fig. 1. Solubilization of synaptic membranes with Triton X-100. (A) Schematic representation of synaptic membrane compartments: (1) endocytic zone, (2) intracellular pool, and (3) active zone. Blue bars, N-cadherin; squares (green, orange, purple), N-cadherin-binding proteins. (B) Crude synaptosome fraction isolated from murine hippocampus was sequentially extracted with 20 mM methyl-β-cyclodextrin (CD), 5 M urea (U), 1% Triton X-100 (T), and SDS-sample buffer (P), followed by SDS–PAGE and Coomassie Brilliant Blue staining. (C) Western blot of the sequentially extracted synaptosome fractions probed with anti-N-cadherin antibody. (D) N-cadherin acquires resistance to trypsin upon synaptic stimulation both in Triton-soluble and -insoluble fractions. Unstimulated (lanes C) and stimulated (lanes K) neuron cultures were treated with trypsin (0.1%, 10 min) first and then harvested directly in SDS–PAGE sample buffer (Total), or in 1% Triton X-100-containing buffer for extraction (TX-sol). The Triton-insoluble pellet was resuspended in urea-containing SDS–PAGE sample buffer at room temperature (TX-ins) or at 96 °C (TX-ins + heat), and subjected to western blot. The protected cytoplasmically disposed fragments of partially digested molecules (fragment 1 and 2) as well as intact molecules (full-length) were detected with an antibody recognizing the intracellular domain of N-cadherin. In total neuronal lysates, stimulation (K) induced the increment of the protected full-length N-cadherin and the partially protected fragment 1. In Triton-treated lysates, full-length molecule was not detectable, but the partially protected fragment 1 was increased after the synaptic stimulation.

experiments, specific binding proteins were identified by subtracting control IgG-bound items from N-cadherin-bound items (Table 2).

3.2. Actin cytoskeleton-associated proteins

In addition to immunoglobulin and N-cadherin, two major bands of about 102 and 97 kDa were co-immunoprecipitated and these were identified as αN- and β-catenins, respectively (Table 1, band 7–8). The carboxyl-terminus of N-cadherin is known to be linked to actin cytoskeleton bridged with β- and α-catenins as well as through interactions with various actin-binding proteins such as spectrins (Nelson et al., 1990; Pradhan et al., 2001) and actinins (Knudsen et al., 1995; Nieset et al., 1997). Our results confirmed this as band 2 contained abundant α- and β-spectrins and band 7 contained α-actinin-4 (Table 1). It should be noted that spectrins showed some non-specific binding to the control IgG. However, the intensity of band 2, which mainly contained spectrins, was much higher for N-cadherin than the control IgG (Fig. 2), suggesting that the binding was at least in part specific.

In the shotgun analyses, we identified α- and β-subunits of Na^+/K^+-ATPase (Table 2). In epithelial cells Na^+/K^+-ATPase is known to link plasma membrane to the cortical actin filament network through ankyrin and spectrins (Koob et al., 1988; Morrow et al., 1989; Nelson and Veshnock, 1987). More directly, McNeill and colleagues have demonstrated that uvomorulin (E-cadherin) recruits Na^+/K^+-ATPase and spectrin to the basolateral membrane in a cytoplasmic domain-dependent manner (McNeill et al., 1990). We could not determine whether the linkage of N-cadherin to Na^+/K^+-ATPase exists in neurons or only in glial cells because Na^+/K^+-ATPase was only found in hippocampal extracts and not in cultured neuronal extracts. We also found α-integrin in band 5 (Table 1). A transmembrane cell adhesion molecule, α-integrin, forms a heterodimer with β-integrin, which in turn binds to α-actinin (Otey et al., 1990). Taken together, N-cadherin anchors the cortical actin-associated network involving α-actinin and spectrins, which bridge to other membrane anchor molecules such as integrins and Na^+/K^+-ATPase (Fig. 3A).

3.3. Intermediate filament-associated proteins

Plakoglobin (also known as junction plakoglobin or γ-catenin) was originally identified as a desmosome component, where it can bind to the cadherin family member, desmoglein I (Mathur et al., 1994). The primary structure of plakoglobin shows a close relationship with β-catenin and, in fact, plakoglobin associates with classic cadherins such as N-cadherin (Sacco et al., 1995). Although plakoglobin can anchor classic cadherins via α-catenin to actin in adherens junctions, it loses this ability when incorporated into desmosomes. This specificity is achieved by mutually exclusive interactions of plakoglobin with α-catenin and desmosomal cadherins (Chitaev et al., 1998). On the other hand, the binding of β-catenin and plakoglobin to the common N-cadherin cytoplasmic domain in a mutually exclusive manner (Nathke et al., 1994) raises the possibility of competition between these proteins for N-cadherin. For example, high expression of exogenous plakoglobin can efficiently displace endogenous β-catenin from adherens junctions (Sacco et al., 1995; Salomon et al., 1997). Similarly, in plakoglobin-knockout mice, β-catenin is incorporated into desmosomes, which are normally devoid of this protein (Bierkamp et al., 1999).

In the present study, in addition to β-catenin (band 8), plakoglobin was simultaneously bound to N-cadherin (band 10) (Table 1). This finding was confirmed in hippocampal shotgun analysis (Table 2). Furthermore, desmoplakin, which serves as a bridge

Table 1
Proteins identified in SDS-gel bands with applied N-cadherin-immunoprecipitate.

Description	Mascot score	Accession[a]	Confirm[b]
Band 1			
DYHC1; cytoplasmic dynein 1 heavy chain 1	98.26	729378	Ref.
Band 2			
SPTA2; spectrin alpha chain, brain	190.27	17380501	Ref.
Non-erythrocyte beta-spectrin	10.15	13430206	Ref.
Sptbn1 protein	10.14	60422766	Ref.
Band 3			
Protein for IMAGE:9026960; sperm-associated antigen 9	28.20	197245955	CR
Sperm-associated antigen 9	10.16	157819127	CR
Band 4			
Clathrin, heavy chain (Hc)	180.28	9506497	NS
CADH2; cadherin-2; neural cadherin; N-cadherin; CD325	50.26	13431334	–
Protein for IMAGE:9026960; sperm-associated antigen 9	10.23	197245955	CR
Similar to tripartite motif protein 33	20.22	62644337	CR
Band 5			
rCG36779; ARVCF	50.27	149019791	Ref.
CADH2; cadherin-2; neural cadherin; N-cadherin; CD325	30.24	13431334	–
Amphiphysin	10.18	11560002	ND
Integrin alpha chain	10.12	56393	ND
Catenin (cadherin-associated protein), alpha 2	10.07	157817081	Ref.
Pumilio homolog 1	10.10	157822487	ND
Band 6			
DDB1; DNA damage-binding protein 1	50.32	81868411	NS
Catenin (cadherin-associated protein), alpha 2	140.28	157817081	Ref.
Catenin (cadherin-associated protein), alpha 1, 102 kDa	34.23	55742755	Ref.
Damage-specific DNA-binding protein 1	10.17	149062405	NS
Phosphorylase kinase, beta	10.16	62079039	ND
Band 7			
Catenin (cadherin-associated protein), alpha 1, 102 kDa	320.35	55742755	Ref.
Catenin (cadherin-associated protein), alpha 2	200.29	157817081	Ref.
B39529 cadherin-associated protein, 102 K - rat (fragments)	10.24	92036	Ref.
Similar to catenin delta-2 (NPRAP) (neurojungin)	10.24	109464562	Ref.
rCG38081 (tRNA-binding, unknown function)	8.12	149055468	ND
Alpha-actinin 4	10.16	6636119	Ref.
Beta-catenin	10.16	46048609	Ref.
Band 8			
Beta-catenin	338.34	46048609	Ref.
Catenin (cadherin-associated protein), alpha 1, 102 kDa	30.22	55742755	Ref.
Catenin (cadherin-associated protein), alpha 2	22.15	157817081	Ref.
Cadherin-associated protein, 102 K (fragments)	10.24	92036	Ref.
Valosin-containing protein	10.20	17865351	ND
Proteasome (prosome, macropain) 26S subunit, non-ATPase, 2	10.23	72255509	ND
Band 9			
Beta-catenin	148.29	46048609	Ref.
Catenin (cadherin-associated protein), alpha 1, 102 kDa	20.20	55742755	Ref.
Cadherin-associated protein, 102 K (fragments)	10.22	92036	Ref.
Catenin (cadherin-associated protein), alpha 2	30.18	157817081	Ref.
Band 10			
Heat shock protein 90, alpha (cytosolic), class A member 1	30.26	28467005	ND
Junction plakoglobin	50.28	41529837	Ref.
Beta-catenin	50.25	46048609	Ref.
TNF-receptor-associated protein 1	10.22	84781723	DN
Annexin A2	10.17	9845234	ND
Dsp protein; desmoplakin	10.15	67678070	Ref.
Band 11			
Grp75 (DnaK, HSP9)	30.19	1000439	ND
HNRPM; heterogeneous nuclear ribonucleoprotein M	40.21	71152132	ND
DnaK-type molecular chaperone hsp72-ps1	50.19	347019	ND
Beta-catenin	10.21	46048609	Ref.

Table 1 (*continued*)

Description	Mascot score	Accession[a]	Confirm[b]
Band 13			
Actin, beta-like 2	12.18	157823033	ND
PREDICTED: similar to cellular repressor of E1A-stimulated genes 2	8.07	109485991	ND
Band 14			
Syntaxin 1B2	20.20	6981600	DN
Glyceraldehyde-3-phosphate dehydrogenase	40.20	8393418	DN
Apolipoprotein E	10.15	162287337	ND
PREDICTED: similar to glyceraldehyde-3-phosphate dehydrogenase	10.13	62657298	DN
Hypothetical protein LOC301563 (mitochondrial fission factor)	10.11	84781650	ND
Band 15			
G chain G, rat liver F1-Atpase	30.20	6729936	ND
Vacuolar H + ATPase E1	10.16	38454230	ND
14-3-3 epsilon	40.21	5803225	DN
Band 16			
AF370442_1 LEK1	14.14	14091667	Ref.

[a] Genbank Accession Number.
[b] NS, found non-specific in further experiments; CR, cross reactivity by anti-N-cadherin antibody; DN, binding was denied in further experiments; Ref, confirmed literally; ND, not determined.

Table 2
Proteins identified in shotgun analyses by subtracting IgG-bound items from anti-N-cadherin antibody-bound items.

Description	Mascot score	Accession[a]	Confirm[b]
Cadherins			
Cdh2 cadherin-2	140.28	12558	–
Cdh2 cadherin 2 precursor	20.21	12558	–
Cdh4 cadherin-4	10.12	12561	Ref.
Catenins			
Ctnnb1 catenin beta-1	210.35	12387	Ref.
Ctnna2 isoform 1 of catenin alpha-2	110.30	12386	Ref.
Ctnna2 isoform 2 of catenin alpha-2	10.22	12386	Ref.
Ctnnd2 isoform 1 of catenin delta-2	50.21	18163	Ref.
Jup junction plakoglobin	20.25	16480	Ref.
Cytoskeletal/membranous			
Actr3 actin-related protein 3	10.16	74117	Ref.
Spna2 spectrin alpha 2	10.18	20740	Ref.
Atp1b1 sodium/potassium-transporting ATPase subunit beta-1	10.19	11931	Ref.
Atp1a3 sodium/potassium-transporting ATPase subunit alpha-3	10.16	232975	Ref.
Unknown			
BC005561 cDNA sequence BC005561	10.12	100042165	ND
Non-specific			
Spag9 isoform 2 of C-jun-amino-terminal kinase-interacting protein 4	50.24	70834	CR
Trim33 isoform alpha of E3 ubiquitin-protein ligase TRIM33	10.18	94093	CR

[a] Genbank Accession Number.
[b] CR, cross-reactivity with anti-N-cadherin antibody; Ref, confirmed literally; ND, not determined.

between plakoglobin and intermediate filaments in desmosomes (Kowalczyk et al., 1997; Schmidt et al., 1994; Smith and Fuchs, 1998), was also found in band 10 (Table 1). In the case of chick optic tectum, β-catenin and plakoglobin are enriched at synapses and associated with N-cadherin, but they are differentially distributed forming mutually exclusive complexes (Miskevich et al., 1998). Taking this into account, we speculate that plakoglobin/desmoplakin complex might tether intermediate filaments to a certain subset of synaptic junctions whose adhesion is mediated by N-cadherin (Fig. 3B).

3.4. Proteins tethering microtubules

In our immunoprecipitate, there was abundant cytoplasmic dynein heavy chain 1 in band 1 (Table 1). In addition, band 16 included LEK1/CENPF/mitosin, which is known to associate with dynein bridged with NudE1/LIS1 (Soukoulis et al., 2005). It has been reported that cytoplasmic dynein binds to β-catenin at the cell cortex where E-cadherin forms adherens junction with the neighboring cell (Ligon et al., 2001). Microtubules (MT) are tethered by this cadherin-β-catenin-dynein complex at the adherens junction and facilitate junction assembly (Ligon and Holzbaur, 2007). It has also been proposed that LIS1 interacts with IQGAP1, a β-catenin-binding partner, and a Rho-family GTPase Cdc42 in a calcium-dependent manner (Kholmanskikh et al., 2006).

Transportation of N-cadherin to plasma membrane is consistently dependent on MT networks as well as MT-based motors (Mary et al., 2002; Teng et al., 2005). Recent studies have shown that MT plus-ends terminate at the adherens junctions of mammary tumor cells and that MT depolymerization causes

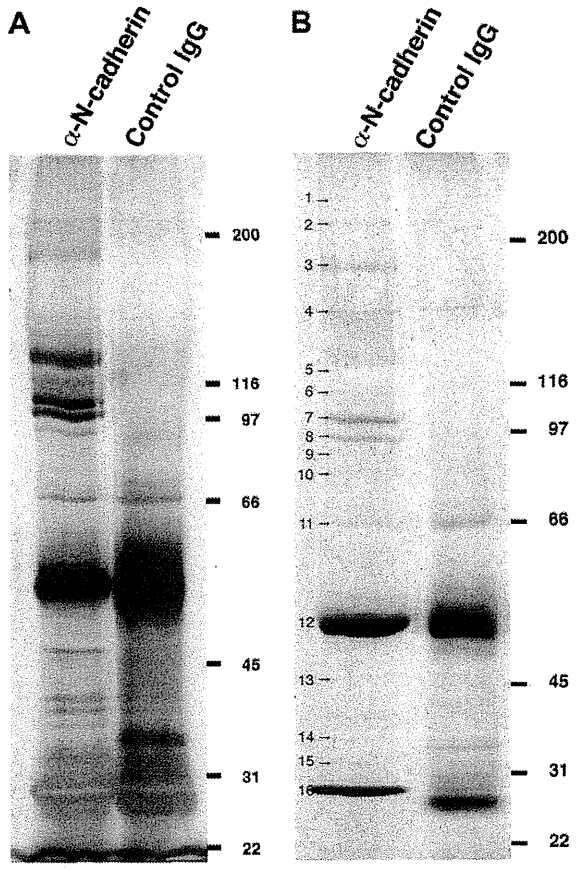

Fig. 2. Immunoprecipitation from the Triton X-100 extracts of cultured rat hippocampal neurons. (A) Silver staining. (B) Sypro Ruby staining. Numbers correspond to the bands excised and subjected to in-gel digestion–LC–MS/MS (Table 1).

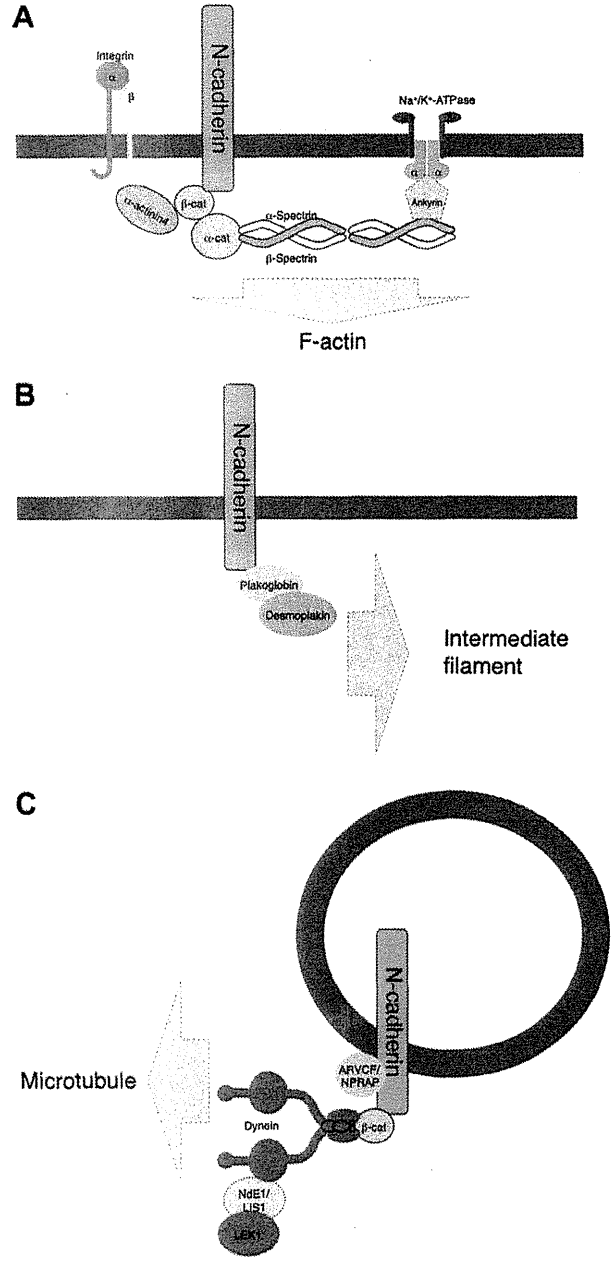

Fig. 3. Models of N-cadherin-associated cell machineries connected to cytoskeletal elements.

disorganized accumulation of E-cadherin in these cells (Stehbens et al., 2006), as observed earlier with other cells (Waterman-Storer et al., 2000). The M-cadherin–catenin complex also interacts with MTs (Kaufmann et al., 1999). Although most of these studies suggest that MT plus-ends interact with cell junctions, one study reported that N-cadherin-mediated adhesion stabilizes the minus-ends (Chausovsky et al., 2000). There is another study which showed that adherens junction is tethered via PLEKHA7/Nezha to MT minus-ends (Meng et al., 2008). Our data suggest that, in hippocampal neurons, N-cadherin is more dominantly tethered to MT plus-ends via β-catenin-dynein than to minus-ends.

MTs have not been considered as being able to enter dendritic spines or to play a role in spine development or dynamics, probably because of dynamic instability at the plus-end within spines. Recent advances in imaging techniques for visualizing MTs in living neurons, however, have revealed that MTs transiently invade into and, therein, are involved in activity-induced spine dynamism and spine development (Gu et al., 2008; Hu et al., 2008). These transient invasions of MTs are correlated with the transient emergence of protrusions on spine heads (transient spine head protrusion: tSHP) (Hu et al., 2008). Interestingly, inactivation of N-cadherin activity in dendritic spines drastically enhances the protrusions of activity-induced tSHPs, as we have previously observed (Okamura et al., 2004). This seems to be consistent with the idea that the N-cadherin-β-catenin-dynein complex tether MT plus-ends and regulate the growth of MTs in the close proximity to synaptic junctions. Taken together, the co-ordination of F-actin and MT at the N-cadherin-mediated synaptic junction is important for activity-induced remodeling of synaptic junctions (Fig. 3C) (Okamura et al., 2004).

3.5. p120ctn family at the juxta-membrane domain

p120ctn family proteins, which bind to the juxta-membrane cytoplasmic domain of classic cadherins, serve as another pathway connected to MTs in non-neuronal tissues (Chen et al., 2003; Franz and Ridley, 2004; Ichii and Takeichi, 2007; Yanagisawa et al., 2004). Among various p120ctn family members, p120ctn/δ1-catenin is involved in synapse development (Elia et al., 2006) and is expressed in cultured hippocampal neurons (Fig. 4). However, N-cadherin-immunoprecipitate did not include

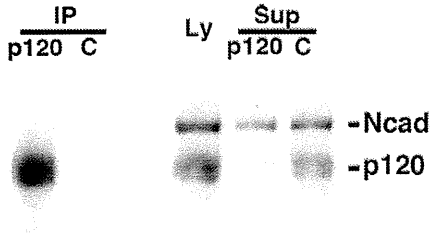

Fig. 4. Immunoprecipitation of p120ctn. Neuronal lysate was immunoprecipitated with anti-p120ctn antibody (p120) or control IgG (C). Ten percent of the lysate (Ly) and flow through (Sup) were also electrophoresed. The transferred membrane was probed with both anti-N-cadherin and anti-p120ctn antibodies.

p120ctn in either in-gel digestion or shotgun analyses (Tables 1 and 2). Western blot following the immunoprecipitation of p120ctn also failed to detect N-cadherin (Fig. 4). On the other hand, ARVCF and NPRAP (neurojungin, δ2-catenin) were found in bands 5 and 7, and in the results of shotgun analysis (Tables 1 and 2). Other family members, plakophilins 1–3 and p0071 (plakophilin 4) were not found. These results are reasonable in that δ2-catenin has been shown to be important for cognitive and synaptic function (Israely et al., 2004) and that learning disabilities are evident in velo-cardio-facial syndrome (Shprintzen et al., 1978; Sirotkin et al., 1997). It has also been suggested that NPRAP is responsible for the synaptic anchorage of AMPA receptor to N-cadherin (Silverman et al., 2007). An actin polymerization protein, actin-related protein 3 (Actr3) was found in the shotgun analysis (Table 2). It has also been reported that the p120ctn family binds to cortactin, which in turn binds to Arp3 (Boguslavsky et al., 2007). In the Xenopus system there is an alternative pathway that links ARVCF with spectrin via kazrin (Cho et al., 2010). Taken together, ARVCF and NPRAP are the dominant p120ctn family members that form complexes with N-cadherin in hippocampal neurons (Fig. 3C).

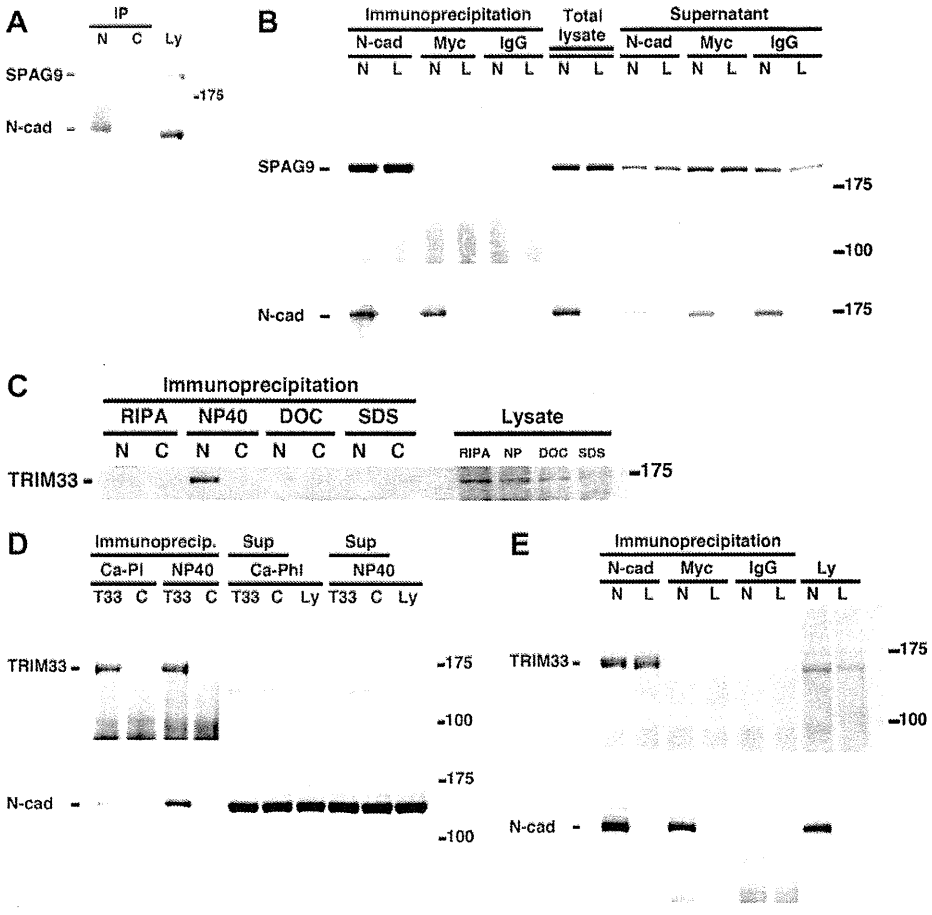

Fig. 5. False positive cases due to the cross-reactivity of anti-N-cadherin antibody were ruled out by rigorous examination. (A) N-cadherin was immunoprecipitated from neuronal lysate and immunoblotted for SPAG9 (top) and N-cadherin (bottom). Immunoprecipitate with anti-N-cadherin antibody (N), with control IgG (C), and 10% of lysate (Ly) were applied. (B) L929 fibroblast cells (L) and those stably transfected with myc-tagged N-cadherin (N) were extracted and immunoprecipitated with anti-N-cadherin (N-cad), anti-myc-tag (myc) antibodies, and control IgG (IgG). The immunoprecipitates, total cell lysates and flow through (supernatant) were immunoblotted with anti-SPAG9 (top) and anti-N-cadherin (bottom) antibodies. (C) Neurons were extracted and immunoprecipitated in the indicated buffer conditions: RIPA (20 mM Tris–HCl (pH 8.0), 150 mM NaCl, 1 mM EDTA, 1% Nonidet P-40, 0.5% sodium deoxycholate, 0.1% SDS, 10 μg/ml leupeptin, 10 μg/ml pepstatin A, 1 μg/ml aprotinin, and 0.2 mM phenylmethylsulfonyl fluoride); NP40 (same without sodium deoxycholate or SDS); DOC (without SDS); SDS (without sodium deoxycholate). The immunoprecipitate with anti-N-cadherin antibody (N), with control IgG (C), and 10% of total lysate were immunoblotted with anti-TRIM33 antibody. (D) Neurons were extracted and immunoprecipitated with anti-TRIM33 antibody in Ca-PI-lysis buffer or NP40 buffer. The immunoprecipitate with anti-TRIM33 antibody (T33), with control IgG (C), flow through (Sup), and 10% of total lysate (Ly) were immunoblotted with anti-TRIM33 antibody (top) and anti-N-cadherin antibody (bottom). E, L929 fibroblast cells (L) and those stably transfected with myc-tagged N-cadherin (N) were extracted and immunoprecipitated with anti-N-cadherin (N-cad), anti-myc-tag (myc) antibodies, and control IgG (IgG). The immunoprecipitates and total cell lysates (Ly) were immunoblotted with anti-TRIM33 antibody (top) and anti-N-cadherin antibody (bottom).

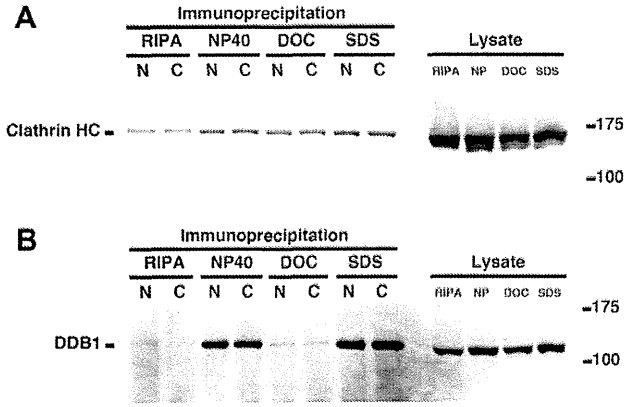

Fig. 6. Non-specific binding cases revealed by immunoblotting. Neurons were extracted and immunoprecipitated in the indicated buffer conditions. The immunoprecipitate with anti-N-cadherin antibody (N), with control IgG (C), and 10% of total lysate were immunoblotted with anti-clathrin heavy chain (A) and anti-DDB1 (B) antibodies.

3.6. Implications for the interactions with specific membrane compartments

Band 10 contained annexin A2, a calcium-dependent membrane-associated protein complexed with p11 (Table 1). In HUVEC cells, the annexin A2/p11 heterotetramer complex, which accumulates underneath the plasma membrane at cholesterol raft sites, is associated with VE-cadherin, although there was no association with N-cadherin (Heyraud et al., 2008). This interaction is probably involved in the stabilization of cadherin–catenin complex at the forming adherens junction. The binding of annexin A2 to N-cadherin found in the present setting therefore suggests that synaptic dynamism involves the stabilization and destabilization of the synaptic junction via interaction with the lipid raft-associated cell machinery.

Furthermore, the inclusion of amphiphysin, a BAR domain protein to form membrane curvature, may reflect the involvement of N-cadherin in the curved membrane such as that of the endosome (Table 1, band 5). A *Caenorhabditis elegans* F-BAR domain protein SRGP-1 is also reported to co-localize with cadherin–catenin complex (HMR-1 and HMP-1) in the adherens junction and SRGP-1 loss-of-function results in a compromised cadherin–catenin complex (Zaidel-Bar et al., 2010).

3.7. Assessment of unreported proteins

In addition to the previously reported N-cadherin-binding partners, there were several proteins that were apparently specific for N-cadherin compared to IgG control (Fig. 2A). For example, band 3 showed highly specific affinity for N-cadherin and included sperm associated antigen 9 (SPAG9) (Table 1). SPAG9 were also found in band 4 (Table 1) and in shotgun analysis (Table 2). This apparently specific binding of SPAG9 to N-cadherin was reproduced by immunoblotting following immunoprecipitation (Fig. 5A). However, immunoprecipitation of SPAG9 was observed from L929 cells with or without the expression of N-cadherin. Moreover, anti-myc tag antibody did not precipitate SPAG9 from the cells transfected with recombinant N-cadherin fused with myc-tag (Fig. 5B). These data indicate that the anti-N-cadherin antibody directly cross-reacts with SPAG9, so there is no intrinsic association of SPAG9 with N-cadherin.

Cross-reactivity was also the case for tripartite motif protein 33 (TRIM33) found in band 4 and in shotgun analysis (Tables 1 and 2). In immunoblot analyses, the apparent binding of TRIM33 was specific and sensitive to ionic detergent treatment, such as sodium deoxycholate and SDS (Fig. 5C and D). Immunoprecipitation of L929 cells with or without N-cadherin-myc revealed that the anti-N-cadherin antibody was directly bound to TRIM33 (Fig. 5E).

Clathrin heavy chain was abundant in band 3 (Table 1). In the immunoblot analysis, this binding was found to be non-specific (Fig. 6A). Similarly, DNA damage-binding protein 1 (DDB1)/damage-specific DNA-binding protein 1 found in band 6 turned out to be non-specific (Fig. 6B). These non-specific signals were successfully ruled out in shotgun analysis by subtracting the non-specific binders (control IgG) from the specific binders.

Band 14 included syntaxin 1B2 and glyceraldehyde-3-phosphate dehydrogenase, and band 10 included TNF receptor associated protein 1 (TRAP1) (Table 1). The co-immunoprecipitation of these proteins has not been detectable in our immunoblottings so far (Fig. 7).

3.8. Dynamism of the adhesion complex upon synaptic stimulation

N-cadherin expressed in developed brain is distributed to specific synaptic contacts and has been implicated in the formation and maintenance of the CNS synaptic junction (Benson and Tanaka, 1998; Fannon and Colman, 1996; Togashi et al., 2002). However, N-cadherin in CNS is now appreciated as a dynamic regulator of synaptic structure and function, responding instantly to synaptic activity (Bozdagi et al., 2004, 2010; Jungling et al., 2006; Mendez et al., 2010; Okamura et al., 2004; Tanaka et al., 2000). The activation of the NMDA receptor results in the dephosphorylation of β-catenin at Tyr-654. The dephosphorylated β-catenin is recruited to the cytoplasmic domain of N-cadherin and stabilizes it on the cell surface (Murase et al., 2002; Tai et al., 2007). At the same time, N-cadherin itself shows stabilized conformation as demonstrated by its super-resistance to extracellular trypsin and its stable dimer in SDS-gels (Tanaka et al., 2000). We reasoned that such a change

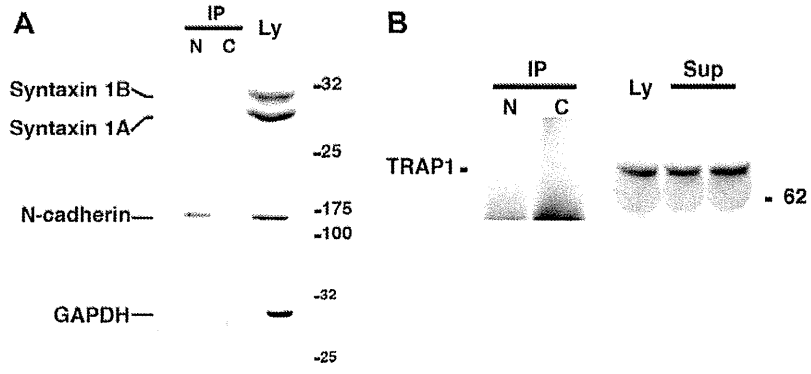

Fig. 7. Non-reproducible cases in immunoblotting. Neurons were extracted and immunoprecipitated with anti-N-cadherin antibody. The immunoprecipitate with anti-N-cadherin antibody (N), with control IgG (C), 10% of total lysate (Ly), and flow through (Sup), were immunoblotted with anti-syntaxin 1 (A, top), anti-N-cadherin (A, middle), anti-GAPDH (A, bottom), and anti-TRAP1 (B) antibodies.

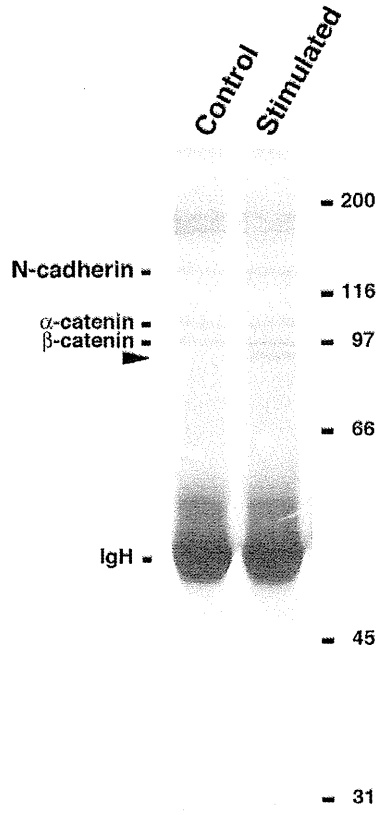

Fig. 8. Synaptic stimulation induces a change in the profile of N-cadherin immunoprecipitates. Control (left) or depolarized (50 mM K^+, 15 min; right) rat hippocampal neurons were extracted with Ca-PI lysis buffer and immunoprecipitated with anti-N-cadherin antibody. IgH: Immunoglobulin heavy chain. Arrowhead indicates a band specifically intensified in the stimulated neurons.

in N-cadherin conformation accompanies alterations of N-cadherin-binding proteins.

The immunoprecipitation of N-cadherin from neurons depolarized for 15 min showed a stronger 93-kDa band than from non-stimulated neurons (Fig. 8). This band corresponded to band 9, which included a shorter variant of α2-catenin and a fragment of β-catenin (Table 1). It has been reported that NMDA-receptor activation yields an increase in shorter β-catenin immunoreactivity around this molecular size (85 kDa) via the cleavage of full-length β-catenin by activated calpain (Abe and Takeichi, 2007). Although the calpain-cleaved β-catenin fragment is released from N-cadherin, the 93-kD β-catenin maintained its association with N-cadherin under our experimental conditions, probably because it maintains the binding domain to N-cadherin. Our immunoprecipitation buffer contained 1% Triton X-100, but without any ionic detergent, and was mild enough to maintain relatively weak protein–protein interactions. N-cadherin-binding domain is consistently preserved in the N-terminal-truncated fragment (Kemler, 1993; Sacco et al., 1995); calpain cleaves the N-terminal 28–30 amino acid fragment of β-catenin (Abe and Takeichi, 2007). The significant enhancement of truncated β-catenin observed in silver-stained gel suggests that the regulation of N-cadherin adhesivity by this modification of β-catenin is a major mechanism underlying synaptic remodeling.

Acknowledgements

We thank Shi Hong for technical assistance. This work was supported by Grants-in-Aid for Scientific Research from the Ministry of Education, Culture, Sports, Science and Technology, Japan to H.T. and Y.K.; and the Takeda Science Foundation and the Japan Foundation for Applied Enzymology to H.T.

References

Abe, K., Takeichi, M., 2007. NMDA-receptor activation induces calpain-mediated beta-catenin cleavages for triggering gene expression. Neuron 53, 387–397.
Bamji, S.X., Rico, B., Kimes, N., Reichardt, L.F., 2006. BDNF mobilizes synaptic vesicles and enhances synapse formation by disrupting cadherin-beta-catenin interactions. J. Cell Biol. 174, 289–299.
Bamji, S.X., Shimazu, K., Kimes, N., Huelsken, J., Birchmeier, W., Lu, B., Reichardt, L.F., 2003. Role of beta-catenin in synaptic vesicle localization and presynaptic assembly. Neuron 40, 719–731.
Benson, D.L., Tanaka, H., 1998. N-cadherin redistribution during synaptogenesis in hippocampal neurons. J. Neurosci. 18, 6892–6904.
Bierkamp, C., Schwarz, H., Huber, O., Kemler, R., 1999. Desmosomal localization of beta-catenin in the skin of plakoglobin null-mutant mice. Development 126, 371–381.
Boguslavsky, S., Grosheva, I., Landau, E., Shtutman, M., Cohen, M., Arnold, K., Feinstein, E., Geiger, B., Bershadsky, A., 2007. P120 catenin regulates lamellipodial dynamics and cell adhesion in cooperation with cortactin. Proc. Natl. Acad. Sci. USA 104, 10882–10887.
Bozdagi, O., Shan, W., Tanaka, H., Benson, D.L., Huntley, G.W., 2000. Increasing numbers of synaptic puncta during late-phase LTP: N-cadherin is synthesized, recruited to synaptic sites, and required for potentiation. Neuron 28, 245–259.
Bozdagi, O., Valcin, M., Poskanzer, K., Tanaka, H., Benson, D.L., 2004. Temporally distinct demands for classic cadherins in synapse formation and maturation. Mol. Cell. Neurosci. 27, 509–521.
Bozdagi, O., Wang, X.B., Nikitczuk, J.S., Anderson, T.R., Bloss, E.B., Radice, G.L., Zhou, Q., Benson, D.L., Huntley, G.W., 2010. Persistence of coordinated long-term potentiation and dendritic spine enlargement at mature hippocampal CA1 synapses requires N-cadherin. J. Neurosci. 30, 9984–9989.
Brown, D.A., Rose, J.K., 1992. Sorting of GPI-anchored proteins to glycolipid-enriched membrane subdomains during transport to the apical cell surface. Cell 68, 533–544.
Chausovsky, A., Bershadsky, A.D., Borisy, G.G., 2000. Cadherin-mediated regulation of microtubule dynamics. Nat. Cell Biol. 2, 797–804.
Chen, X., Kojima, S., Borisy, G.G., Green, K.J., 2003. P120 catenin associates with kinesin and facilitates the transport of cadherin–catenin complexes to intercellular junctions. J. Cell Biol. 163, 547–557.
Chitaev, N.A., Averbakh, A.Z., Troyanovsky, R.B., Troyanovsky, S.M., 1998. Molecular organization of the desmoglein-plakoglobin complex. J. Cell Sci. 111 (Pt 14), 1941–1949.
Cho, K., Vaught, T.G., Ji, H., Gu, D., Papasakelariou-Yared, C., Horstmann, N., Jennings, J.M., Lee, M., Sevilla, L.M., Kloc, M., Reynolds, A.B., Watt, F.M., Brennan, R.G., Kowalczyk, A.P., McCrea, P.D., 2010. Xenopus Kazrin interacts with ARVCF-catenin, spectrin and p190B RhoGAP, and modulates RhoA activity and epithelial integrity. J. Cell Sci. 123, 4128–4144.
Cotman, C.W., Banker, G., Churchill, L., Taylor, D., 1974. Isolation of postsynaptic densities from rat brain. J. Cell Biol. 63, 441–455.
Elia, L.P., Yamamoto, M., Zang, K., Reichardt, L.F., 2006. P120 catenin regulates dendritic spine and synapse development through Rho-family GTPases and cadherins. Neuron 51, 43–56.
Fannon, A.M., Colman, D.R., 1996. A model for central synaptic junctional complex formation based on the differential adhesive specificities of the cadherins. Neuron 17, 423–434.
Fischer, M., Kaech, S., Wagner, U., Brinkhaus, H., Matus, A., 2000. Glutamate receptors regulate actin-based plasticity in dendritic spines. Nat. Neurosci. 3, 887–894.
Franz, C.M., Ridley, A.J., 2004. P120 catenin associates with microtubules: inverse relationship between microtubule binding and Rho GTPase regulation. J. Biol. Chem. 279, 6588–6594.
Fukazawa, Y., Saitoh, Y., Ozawa, F., Ohta, Y., Mizuno, K., Inokuchi, K., 2003. Hippocampal LTP is accompanied by enhanced F-actin content within the dendritic spine that is essential for late LTP maintenance in vivo. Neuron 38, 447–460.
Gu, J., Firestein, B.L., Zheng, J.Q., 2008. Microtubules in dendritic spine development. J. Neurosci. 28, 12120–12124.
Heyraud, S., Jaquinod, M., Durmort, C., Dambroise, E., Concord, E., Schaal, J.P., Huber, P., Gulino-Debrac, D., 2008. Contribution of annexin 2 to the architecture of mature endothelial adherens junctions. Mol. Cell. Biol. 28, 1657–1668.
Hu, X., Viesselmann, C., Nam, S., Merriam, E., Dent, E.W., 2008. Activity-dependent dynamic microtubule invasion of dendritic spines. J. Neurosci. 28, 13094–13105.
Ichii, T., Takeichi, M., 2007. P120-catenin regulates microtubule dynamics and cell migration in a cadherin-independent manner. Genes Cells 12, 827–839.
Israely, I., Costa, R.M., Xie, C.W., Silva, A.J., Kosik, K.S., Liu, X., 2004. Deletion of the neuron-specific protein delta-catenin leads to severe cognitive and synaptic dysfunction. Curr. Biol. 14, 1657–1663.
Jungling, K., Eulenburg, V., Moore, R., Kemler, R., Lessmann, V., Gottmann, K., 2006. N-cadherin transsynaptically regulates short-term plasticity at glutamatergic synapses in embryonic stem cell-derived neurons. J. Neurosci. 26, 6968–6978.

Kaufmann, U., Kirsch, J., Irintchev, A., Wernig, A., Starzinski-Powitz, A., 1999. The M-cadherin catenin complex interacts with microtubules in skeletal muscle cells: implications for the fusion of myoblasts. J. Cell Sci. 112 (Pt 1), 55–68.
Kemler, R., 1993. From cadherins to catenins: cytoplasmic protein interactions and regulation of cell adhesion. Trends Genet. 9, 317–321.
Kholmanskikh, S.S., Koeller, H.B., Wynshaw-Boris, A., Gomez, T., Letourneau, P.C., Ross, M.E., 2006. Calcium-dependent interaction of Lis1 with IQGAP1 and Cdc42 promotes neuronal motility. Nat. Neurosci. 9, 50–57.
Knudsen, K.A., Soler, A.P., Johnson, K.R., Wheelock, M.J., 1995. Interaction of alpha-actinin with the cadherin/catenin cell-cell adhesion complex via alpha-catenin. J. Cell Biol. 130, 67–77.
Koob, R., Zimmermann, M., Schoner, W., Drenckhahn, D., 1988. Colocalization and coprecipitation of ankyrin and Na+, K+-ATPase in kidney epithelial cells. Eur. J. Cell Biol. 45, 230–237.
Kowalczyk, A.P., Bornslaeger, E.A., Borgwardt, J.E., Palka, H.L., Dhaliwal, A.S., Corcoran, C.M., Denning, M.F., Green, K.J., 1997. The amino-terminal domain of desmoplakin binds to plakoglobin and clusters desmosomal cadherin-plakoglobin complexes. J. Cell Biol. 139, 773–784.
Ligon, L.A., Holzbaur, E.L., 2007. Microtubules tethered at epithelial cell junctions by dynein facilitate efficient junction assembly. Traffic 8, 808–819.
Ligon, L.A., Karki, S., Tokito, M., Holzbaur, E.L., 2001. Dynein binds to beta-catenin and may tether microtubules at adherens junctions. Nat. Cell Biol. 3, 913–917.
Lin, B., Kramar, E.A., Bi, X., Brucher, F.A., Gall, C.M., Lynch, G., 2005. Theta stimulation polymerizes actin in dendritic spines of hippocampus. J. Neurosci. 25, 2062–2069.
Luo, J., Wang, Y., Yasuda, R.P., Dunah, A.W., Wolfe, B.B., 1997. The majority of *N*-methyl-D-aspartate receptor complexes in adult rat cerebral cortex contain at least three different subunits (NR1/NR2A/NR2B). Mol. Pharmacol. 51, 79–86.
Manabe, T., Togashi, H., Uchida, N., Suzuki, S.C., Hayakawa, Y., Yamamoto, M., Yoda, H., Miyakawa, T., Takeichi, M., Chisaka, O., 2000. Loss of cadherin-11 adhesion receptor enhances plastic changes in hippocampal synapses and modifies behavioral responses. Mol. Cell. Neurosci. 15, 534–546.
Mary, S., Charrasse, S., Meriane, M., Comunale, F., Travo, P., Blangy, A., Gauthier-Rouviere, C., 2002. Biogenesis of N-cadherin-dependent cell–cell contacts in living fibroblasts is a microtubule-dependent kinesin-driven mechanism. Mol. Biol. Cell 13, 285–301.
Mathur, M., Goodwin, L., Cowin, P., 1994. Interactions of the cytoplasmic domain of the desmosomal cadherin Dsg1 with plakoglobin. J. Biol. Chem. 269, 14075–14080.
McNeill, H., Ozawa, M., Kemler, R., Nelson, W.J., 1990. Novel function of the cell adhesion molecule uvomorulin as an inducer of cell surface polarity. Cell 62, 309–316.
Mendez, P., De Roo, M., Poglia, L., Klauser, P., Muller, D., 2010. N-cadherin mediates plasticity-induced long-term spine stabilization. J. Cell Biol. 189, 589–600.
Meng, W., Mushika, Y., Ichii, T., Takeichi, M., 2008. Anchorage of microtubule minus ends to adherens junctions regulates epithelial cell–cell contacts. Cell 135, 948–959.
Miskevich, F., Zhu, Y., Ranscht, B., Sanes, J.R., 1998. Expression of multiple cadherins and catenins in the chick optic tectum. Mol. Cell. Neurosci. 12, 240–255.
Morrow, J.S., Cianci, C.D., Ardito, T., Mann, A.S., Kashgarian, M., 1989. Ankyrin links fodrin to the alpha subunit of Na, K-ATPase in Madin-Darby canine kidney cells and in intact renal tubule cells. J. Cell Biol. 108, 455–465.
Murase, S., Mosser, E., Schuman, E.M., 2002. Depolarization drives beta-Catenin into neuronal spines promoting changes in synaptic structure and function. Neuron 35, 91–105.
Nathke, I.S., Hinck, L., Swedlow, J.R., Papkoff, J., Nelson, W.J., 1994. Defining interactions and distributions of cadherin and catenin complexes in polarized epithelial cells. J. Cell Biol. 125, 1341–1352.
Nelson, W.J., Shore, E.M., Wang, A.Z., Hammerton, R.W., 1990. Identification of a membrane-cytoskeletal complex containing the cell adhesion molecule uvomorulin (E-cadherin), ankyrin, and fodrin in Madin-Darby canine kidney epithelial cells. J. Cell Biol. 110, 349–357.
Nelson, W.J., Veshnock, P.J., 1987. Ankyrin binding to (Na+ + K+)ATPase and implications for the organization of membrane domains in polarized cells. Nature 328, 533–536.
Nieset, J.E., Redfield, A.R., Jin, F., Knudsen, K.A., Johnson, K.R., Wheelock, M.J., 1997. Characterization of the interactions of alpha-catenin with alpha-actinin and beta-catenin/plakoglobin. J. Cell Sci. 110 (Pt 8), 1013–1022.
Okamoto, K., Nagai, T., Miyawaki, A., Hayashi, Y., 2004. Rapid and persistent modulation of actin dynamics regulates postsynaptic reorganization underlying bidirectional plasticity. Nat. Neurosci. 7, 1104–1112.
Okamura, K., Tanaka, H., Yagita, Y., Saeki, Y., Taguchi, A., Hiraoka, Y., Zeng, L.H., Colman, D.R., Miki, N., 2004. Cadherin activity is required for activity-induced spine remodeling. J. Cell Biol. 167, 961–972.
Okuda, T., Yu, L.M., Cingolani, L.A., Kemler, R., Goda, Y., 2007. Beta-Catenin regulates excitatory postsynaptic strength at hippocampal synapses. Proc. Natl. Acad. Sci. USA 104, 13479–13484.
Otey, C.A., Pavalko, F.M., Burridge, K., 1990. An interaction between alpha-actinin and the beta 1 integrin subunit in vitro. J. Cell Biol. 111, 721–729.
Phillips, G.R., Huang, J.K., Wang, Y., Tanaka, H., Shapiro, L., Zhang, W., Shan, W.S., Arndt, K., Frank, M., Gordon, R.E., Gawinowicz, M.A., Zhao, Y., Colman, D.R., 2001. The presynaptic particle web: ultrastructure, composition, dissolution, and reconstitution. Neuron 32, 63–77.
Pradhan, D., Lombardo, C.R., Roe, S., Rimm, D.L., Morrow, J.S., 2001. Alpha -Catenin binds directly to spectrin and facilitates spectrin-membrane assembly in vivo. J. Biol. Chem. 276, 4175–4181.
Sacco, P.A., McGranahan, T.M., Wheelock, M.J., Johnson, K.R., 1995. Identification of plakoglobin domains required for association with N-cadherin and alpha-catenin. J. Biol. Chem. 270, 20201–20206.
Saglietti, L., Dequidt, C., Kamieniarz, K., Rousset, M.C., Valnegri, P., Thoumine, O., Beretta, F., Fagni, L., Choquet, D., Sala, C., Sheng, M., Passafaro, M., 2007. Extracellular interactions between GluR2 and N-cadherin in spine regulation. Neuron 54, 461–477.
Salomon, D., Sacco, P.A., Roy, S.G., Simcha, I., Johnson, K.R., Wheelock, M.J., Ben-Ze'ev, A., 1997. Regulation of beta-catenin levels and localization by overexpression of plakoglobin and inhibition of the ubiquitin–proteasome system. J. Cell Biol. 139, 1325–1335.
Schmidt, A., Heid, H.W., Schafer, S., Nuber, U.A., Zimbelmann, R., Franke, W.W., 1994. Desmosomes and cytoskeletal architecture in epithelial differentiation: cell type-specific plaque components and intermediate filament anchorage. Eur. J. Cell Biol. 65, 229–245.
Schrick, C., Fischer, A., Srivastava, D.P., Tronson, N.C., Penzes, P., Radulovic, J., 2007. N-cadherin regulates cytoskeletally associated IQGAP1/ERK signaling and memory formation. Neuron 55, 786–798.
Shprintzen, R.J., Goldberg, R.B., Lewin, M.L., Sidoti, E.J., Berkman, M.D., Argamaso, R.V., Young, D., 1978. A new syndrome involving cleft palate, cardiac anomalies, typical facies, and learning disabilities: velo-cardio-facial syndrome. Cleft Palate J. 15, 56–62.
Silverman, J.B., Restituito, S., Lu, W., Lee-Edwards, L., Khatri, L., Ziff, E.B., 2007. Synaptic anchorage of AMPA receptors by cadherins through neural plakophilin-related arm protein AMPA receptor-binding protein complexes. J. Neurosci. 27, 8505–8516.
Sirotkin, H., O'Donnell, H., DasGupta, R., Halford, S., St Jore, B., Puech, A., Parimoo, S., Morrow, B., Skoultchi, A., Weissman, S.M., Scambler, P., Kucherlapati, R., 1997. Identification of a new human catenin gene family member (ARVCF) from the region deleted in velo-cardio-facial syndrome. Genomics 41, 75–83.
Smith, E.A., Fuchs, E., 1998. Defining the interactions between intermediate filaments and desmosomes. J. Cell Biol. 141, 1229–1241.
Soukoulis, V., Reddy, S., Pooley, R.D., Feng, Y., Walsh, C.A., Bader, D.M., 2005. Cytoplasmic LEK1 is a regulator of microtubule function through its interaction with the LIS1 pathway. Proc. Natl. Acad. Sci. USA 102, 8549–8554.
Star, E.N., Kwiatkowski, D.J., Murthy, V.N., 2002. Rapid turnover of actin in dendritic spines and its regulation by activity. Nat. Neurosci. 5, 239–246.
Stehbens, S.J., Paterson, A.D., Crampton, M.S., Shewan, A.M., Ferguson, C., Akhmanova, A., Parton, R.G., Yap, A.S., 2006. Dynamic microtubules regulate the local concentration of E-cadherin at cell–cell contacts. J. Cell Sci. 119, 1801–1811.
Tai, C.Y., Mysore, S.P., Chiu, C., Schuman, E.M., 2007. Activity-regulated N-cadherin endocytosis. Neuron 54, 771–785.
Tanaka, H., Shan, W., Phillips, G.R., Arndt, K., Bozdagi, O., Shapiro, L., Huntley, G.W., Benson, D.L., Colman, D.R., 2000. Molecular modification of N-cadherin in response to synaptic activity. Neuron 25, 93–107.
Tang, L., Hung, C.P., Schuman, E.M., 1998. A role for the cadherin family of cell adhesion molecules in hippocampal long-term potentiation. Neuron 20, 1165–1175.
Teng, J., Rai, T., Tanaka, Y., Takei, Y., Nakata, T., Hirasawa, M., Kulkarni, A.B., Hirokawa, N., 2005. The KIF3 motor transports N-cadherin and organizes the developing neuroepithelium. Nat. Cell Biol. 7, 474–482.
Togashi, H., Abe, K., Mizoguchi, A., Takaoka, K., Chisaka, O., Takeichi, M., 2002. Cadherin regulates dendritic spine morphogenesis. Neuron 35, 77–89.
Uchida, N., Honjo, Y., Johnson, K.R., Wheelock, M.J., Takeichi, M., 1996. The catenin/cadherin adhesion system is localized in synaptic junctions bordering transmitter release zones. J. Cell Biol. 135, 767–779.
Waterman-Storer, C.M., Salmon, W.C., Salmon, E.D., 2000. Feedback interactions between cell-cell adherens junctions and cytoskeletal dynamics in newt lung epithelial cells. Mol. Biol. Cell 11, 2471–2483.
Yagi, T., Takeichi, M., 2000. Cadherin superfamily genes: functions, genomic organization, and neurologic diversity. Genes Dev. 14, 1169–1180.
Yanagisawa, M., Kaverina, I.N., Wang, A., Fujita, Y., Reynolds, A.B., Anastasiadis, P.Z., 2004. A novel interaction between kinesin and p120 modulates p120 localization and function. J. Biol. Chem. 279, 9512–9521.
Yasuda, S., Tanaka, H., Sugiura, H., Okamura, K., Sakaguchi, T., Tran, U., Takemiya, T., Mizoguchi, A., Yagita, Y., Sakurai, T., De Robertis, E.M., Yamagata, K., 2007. Activity-induced protocadherin arcadlin regulates dendritic spine number by triggering N-cadherin endocytosis via TAO2beta and p38 MAP kinases. Neuron 56, 456–471.
Zaidel-Bar, R., Joyce, M.J., Lynch, A.M., Witte, K., Audhya, A., Hardin, J., 2010. The F-BAR domain of SRGP-1 facilitates cell-cell adhesion during *C. elegans* morphogenesis. J. Cell Biol. 191, 761–769.

Mouse ES cells maintained in different pluripotency-promoting conditions differ in their neural differentiation propensity

Haruka Hirose, Hidemasa Kato, Akie Kikuchi-Taura, Toshihiro Soma & Akihiko Taguchi

In Vitro Cellular & Developmental Biology - Animal

ISSN 1071-2690
Volume 48
Number 3

In Vitro Cell.Dev.Biol.-Animal (2012)
48:143-148
DOI 10.1007/s11626-012-9486-z

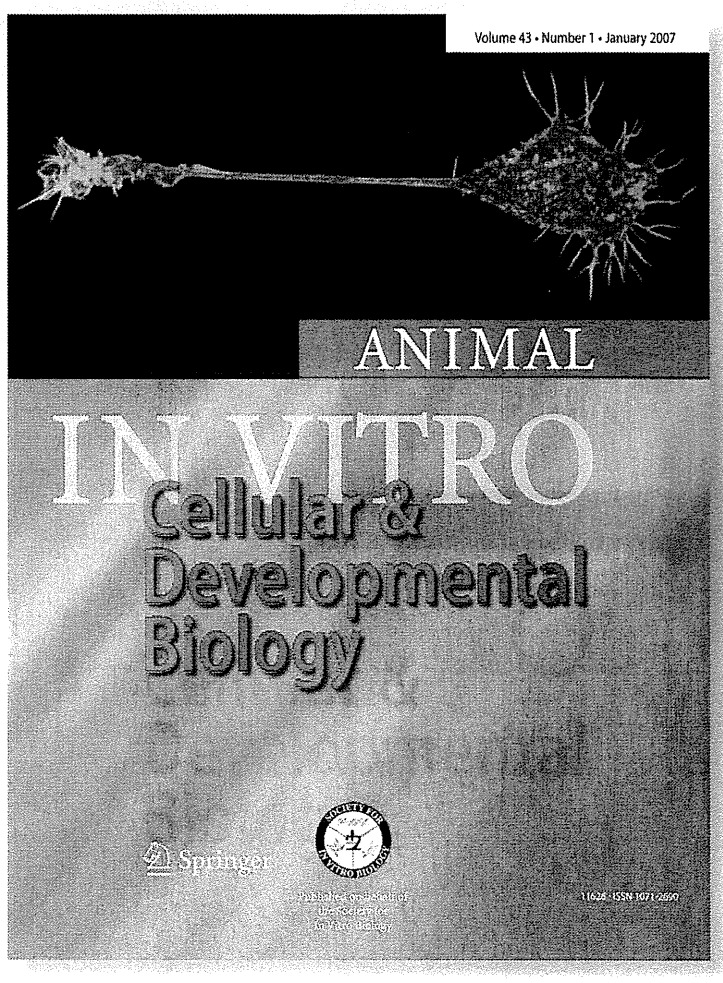

Springer